The Influence of Occupant's Size, Shape and Seat Adjustment in Frontal and Side Impacts

The Influence of Occupant's Size, Shape and Seat Adjustment in Frontal and Side Impacts

Alexandros Leledakis, Jonas Östh, Johan Iraeus, Johan Davidsson, Lotta Jakobsson

Abstract The sensitivity of occupant kinematic and kinetic crash responses to anthropometric and seat adjustment variation was investigated by performing frontal- and side-impact simulations with a family of morphed Human Body Models (HBMs). The HBM family included variations of shape and size, accounting for stature, Body Mass Index (BMI) and sex. A global sensitivity analysis method was developed and applied. Increased BMI was associated with increased spinal and extremity loading in the HBM for all evaluated impacts. Increasing the stature resulted in a consistent increase in lower extremity loading. The fore-aft seat position influenced the head and torso speed relative to the vehicle interior. Furthermore, in high-severity frontal impacts, adjusting the seat position rearwards altered the load path, increasing the HBM pelvic and lumbar spine loading in favour of reducing the lower extremity forces, and vice versa when the seat was positioned forward. The results from this study highlight potential occupant protection challenges and trade-offs, and can be used to enhance protection, considering occupant anthropometric diversity and seat adjustment variation.

Keywords Anthropometric variation, Finite Element, Human Body Model, Morphing, Sensitivity analysis.

I. INTRODUCTION

Car occupants come in a wide range of sizes and shapes, but occupant safety is typically evaluated using a limited set of standardised anthropometries. Numerous studies have found evidence that anthropometric variations can influence the occupant's response during a crash. A matched-pair analysis of field data revealed that obese passengers have 32% higher fatality risk and 40% higher MAIS3+ injury risk [1]. Increased probabilities of extremity and spinal injuries were observed in an analysis of police-reported crashes in the US NASS-CDS database between 2000 and 2015 for higher Body Mass Index (BMI) occupants compared to normal BMI occupants in frontal impacts [2]. Besides the increased injury risks associated with higher BMI occupants, interaction effects between BMI, sex and vehicle type were found [3]. Forman *et al*. [4] found that BMI followed a nonmonotonic relationship, with occupants of lower or higher BMI being more likely to experience AIS3+ thoracic injuries compared to occupants with normal BMI (22–24 kg/m^2). Similarly, a U-shape relation was found between BMI and abdominal injuries in frontal crashes, and different injury patterns were observed between male and female drivers [5]. In a statistical analysis of frontal impacts (NASS-CDS, 1998–2015) [6], female occupants were at greater risk of AIS2+ for most analysed injuries compared to males, with especially large odds ratios (3.05) for the lower extremities. Besides BMI and sex, stature can also influence injury risk, with increased stature being linked to increased odds ratios of MAIS3+ injury risk in far-side impacts [7]. Furthermore, in a comparison of the effects of BMI, sex and age on severe injuries, age was highlighted as having the largest relative contribution to injury risk, especially for the head and thorax [8].

Several simulation studies have been performed to investigate the effect of diverse anthropometries, utilising modelling techniques, such as morphing, and occupant surrogates, such as Human Body Models (HBMs). Parametric Finite Element (FE) HBMs have been developed and utilised in side-impacts to perform sensitivity analysis and to identify parameters influencing occupant response [9]. Preliminary results from the study indicated that body shape affected the impact response more than skeletal and soft tissue material properties. In a more recent simulation study [10], involving 100 HBMs of different age, sex and stature, BMI, stature and shape were reported to affect occupant kinematics, interaction with restraints, and injury risk. BMI was associated with increased lower extremity injury risk, while the neck was not meaningfully affected in the studied

A. Leledakis (e-mail: alexandros.leledakis@chalmers.se; tel.: +46 72 885 2398) is an Industrial PhD student at Chalmers University of Technology and Volvo Cars, Gothenburg, Sweden. J. Östh, PhD, is a Safety Analysis CAE Engineer and L. Jakobsson, PhD, a Senior Technical Leader in Injury Prevention at the Volvo Cars Safety Centre, Gothenburg, Sweden. J. Iraeus, PhD, is a Senior Researcher, J. Davidsson, PhD, an Associate Professor, L. Jakobsson an Adjunct Professor and J. Östh an Adjunct Associate Professor at Chalmers University of Technology, Gothenburg, Sweden. All authors are associated with SAFER – Vehicle and Traffic Safety Centre at Chalmers.

parameter space. In frontal impact simulations [11], increased injury risk for taller and higher BMI occupants was seen in the head and lower extremity region, respectively. Additionally, older occupants had higher thorax and femur injury risk due to lower injury tolerance.

In another simulation study [12], two HBMs were morphed into a wide range of anthropometries and subjected to pendulum thorax impact simulations. The occupant responses, such as chest deflection and peak force, were substantially altered among HBMs with altered anthropometries. Complex nonlinear interaction effects among occupant characteristics were observed, further highlighting the need for considering population diversity during safety evaluations. Similar to the results from field data analysis indicating U-shape responses for occupants of diverse anthropometry [4-5], simulations [13] showed that deviating from average male anthropometry increased the injury risk in frontal impacts. Occupant size was reported [14] as the dominating factor for the injury response, with obese occupants showing an increased likelihood of lower extremity injuries. Besides lower extremity injury risk, obese subjects showed larger hip excursions, which resulted in less forward pitch and could increase submarining risk [15].

In addition to occupant variability, vehicle parameters or adjustments (such as seat adjustment) can also influence the occupant's response. Even though the seat can be adjusted to multiple positions to accommodate occupants of different sizes or increase their comfort level, one study suggests that more than half of all passengers do not alter the seat position when entering a vehicle [16]. As observed in a naturalistic driving study with 75 vehicles [16], the seat was positioned rearward of the mid-travel 92% of the time. Additionally, the mean backrest angle recorded was 25.4° relative to the vertical and remained below 30° in 85% of the frames analysed [16]. Increasing the fore-aft distance can result in increased distance between the Instrument Panel (IP) and driver's knees, which can reduce the lower extremities injury risk [17]. However, it could also alter the occupant loading, affecting the rest of the occupant response.

Generally, reclined backrests have been associated with increased submarining risk, as well as increased lumbar compression loading. In a numerical study of frontal impacts with HBMs of three sizes [18], in which backrest angle and knee bolster position were varied, it was found that increasing the knee-to-bolster distance or the backrest angle resulted in increased submarining risk. Additionally, small occupants had a higher submarining risk. Another simulation study [19], focusing on highly reclined seats, reported that knee bolster could limit the pelvis excursion and increase the torso forward pitch, reducing the submarining risk.

With anthropometric variations and seat adjustment, the belt fit is also affected. The shoulder-belt path was reported to be further forward and inboard for occupants with higher BMI, with larger effects observed for females [20]. In addition to that, the lap-belt was positioned further forward and higher relative to the pelvis [21]. Occupant posture, which has been shown to influence kinematic and kinetic response [22], is also affected by anthropometric parameters, such as stature and BMI [23].

Considering the large influence of occupant anthropometric variability on occupant response, it would be beneficial to develop population-based evaluation methods. Methods [24-25] have been developed that utilise numerical simulation to train meta-models, with the purpose of performing population-based safety evaluations and aiding in vehicle safety development. Although those meta-models can be made to answer specific questions (such as proposing restraint system modification for certain target groups [26]), it would be beneficial to understand the kinematic and kinetic trends present when occupant size and shape are altered. The objective of this study was to investigate, quantify and rank the effect of front-seat passengers' anthropomorphic variation on kinematic and kinetic whole-body responses by simulating a family of HBMs morphed to represent male and female occupants with a wide range of stature and BMI across a wide range of seat adjustments. Frontal and side impacts of varying severity, beyond the scope of standardised testing, were simulated. A systematic analysis of the responses was carried out in the form of sensitivity analysis.

II. METHODS

Four crash pulses were used in a simulation study, with an HBM morphed to represent 22 diverse male and female occupant anthropometries (Fig. 1) in varied seat adjustments. The seat adjustments include changing the fore-aft position across the full range of the travel and using two backrest angles. A full-factorial design was used, leading to 944 in-crash simulations, after excluding the 112 incompatible HBM-seat adjustment combinations (Appendix A, Table A.V). A sensitivity analysis was performed in two steps to quantify the influence of the investigated parameters over occupant's kinematic and kinetic responses.

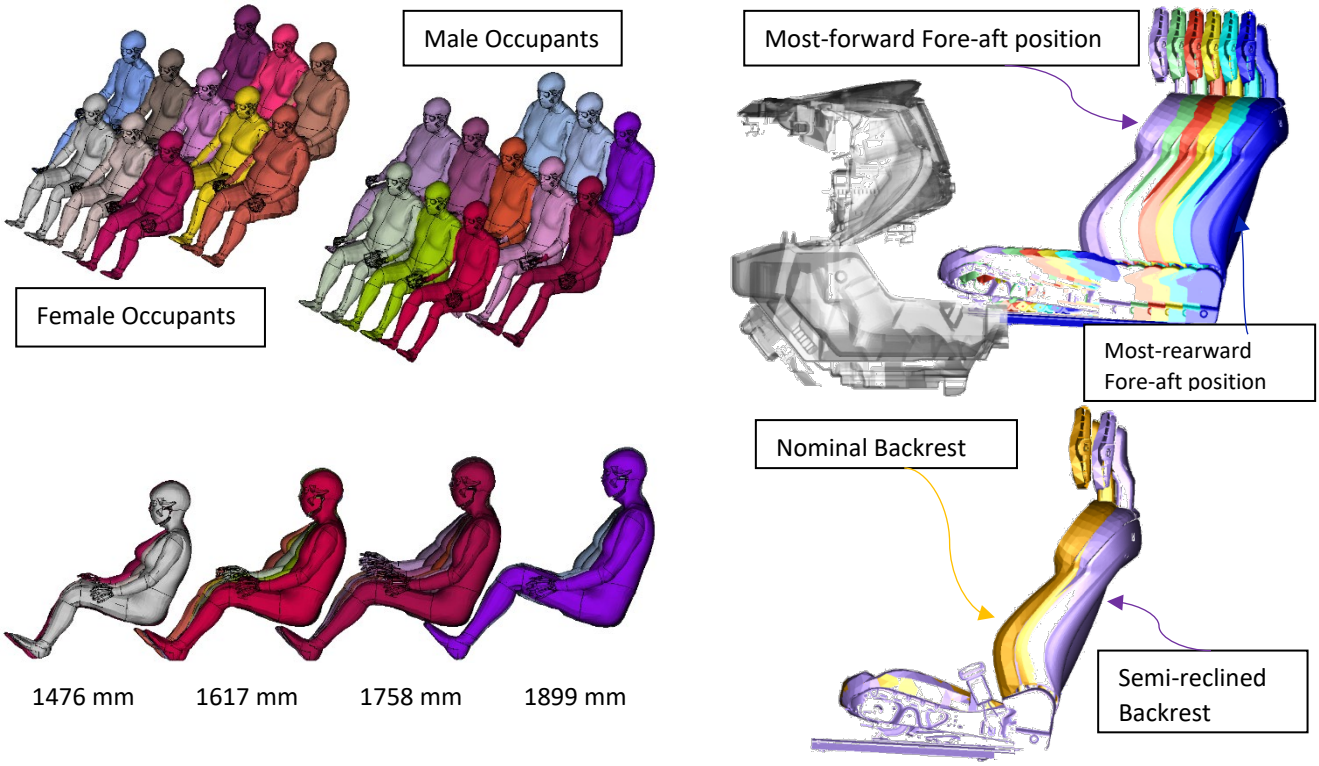

Fig. 1. Overview of the occupant sizes and seat adjustments investigated in this study. On the left, the 11 female and male occupant HBM sizes and, on the right, the seat's fore-aft position and backrest angle are depicted.

Occupant Anthropometry

Data from the National Health and Nutrition Examination Survey (NHANES) for the years 2013–2016 [27], weighted to represent the US population, were analysed to identify the BMI and stature distribution of the population (Appendix A). The medians of the female and male populations (Appendix A, Table A.II) were used as the baseline target anthropometries, while the iso-probability lines [28] covering 90% of the male and female populations were used as the sampling space (Appendix A, Fig. A.2). The occupant's age was kept constant at 40 years old, representing the average age of the injured occupants (Appendix A, Fig. A.1), irrespective of injury level, from the database of the National Automotive Sampling System General Estimates System (NASS GES) between 2011 and 2015 [29]. Using the stature difference between the female and male median stature, an equidistant grid was generated (Fig. A.2), with statures ranging from 1476 mm to 1899 mm, also enabling comparisons of male-female occupants of identical stature and BMI. The median BMI was 28 kg/m^2 and it was varied over 18–38 kg/m^2 while still within the 90% iso-probability lines (Fig. A.2), covering from underweight (<18.5 kg/m^2) up to Obesity Class II (35–40 kg/m^2) occupants, as defined by the World Health Organization (WHO) [30].

Seat Adjustment

The seat was always adjusted at mid-height and low-tilt, while the fore-aft position and the backrest angle were varied. The backrest angle was set to 25° for an upright and 30° for a semi-reclined position (Fig. 1), which matches the mean and 85th percentile backrest angles of the analysed frames in a naturalistic study [16]. Even though the seat fore-aft position is frequently adjusted rearward of the mid-point [16], there could be a need for positioning the seat more forward (e.g. rear-seat occupants or transportation of objects). Therefore, the full range of travel (260 mm) was investigated in steps of 20%, resulting in six positions (Fig. 1), with 0% being defined as the most-forward position and 100% as the most-rearward position.

Numerical Models – Vehicle Interior and Occupant Surrogate

The car occupant was modelled using the SAFER HBM v9.0.1 as the baseline model, which was morphed into target occupant anthropometries (Appendix A, Table A.IV). The baseline HBM [31] represents a 50th percentile male with a stature of 175 cm and weight of 77 kg, and its biofidelity has been evaluated in frontal, near- and far-side impacts [32-36]. The baseline HBM was morphed using an HBM morphing method [34][37] utilising statistical models of the body surface, pelvis, femur, tibia and ribcage towards target anthropometries parametrised for

sex, age, stature and BMI. The morphing method has been evaluated with SAFER HBM v9 in side impacts and has shown improved kinematics prediction compared with the baseline model [34][38].

After the geometric morphing, to match the mass of the target occupant, the HBM's trunk and extremities soft tissue densities were uniformly scaled to achieve the target occupant mass, and the initial length of all discrete muscle elements was reset. Furthermore, the HBM internal contacts were surveyed, and all found intersections were removed by manual movements of soft tissue nodes. The model quality was inspected, and mesh improvements were performed locally when needed while respecting the skeleton part boundaries. After the element quality improvements, the elements violating the defined quality criteria were between 124% and 156% (Appendix A, Table A.IV) compared to the baseline model, with smaller occupants (in stature or BMI) posing more challenges regarding element quality.

A previously validated [22] deformable interior with approximately 2.35 million Finite Elements (FE), contained in a rigid body-in-white, was used to model the vehicle interior of a mid-sized SUV. The HBM was positioned in the front passenger seat and was restrained using models of a three-point pyrotechnically-pretensioned load-limited seatbelt, a frontal passenger airbag (PAB) deploying from the dashboard and, for the side impacts, a seat-mounted torso airbag and an inflatable curtain (IC) (Fig. 3). The restraint system's activation timing was kept constant for all occupant sizes and seat adjustments.

All simulations were performed with the explicit FE solver LS-DYNA MPP s R9.3.0 (ANSYS/LST, Livermore, CA, USA) on the same cluster (using 140 CPUs) to avoid variation due to model decomposition [39]. A right-handed coordinate system (Fig. 3) was used, defined with X rearward, Z upward, and Y toward the vehicle's right side.

Occupant Positioning and Belt Routing

The occupant posture can influence the occupant kinematics [22]. An automated occupant positioning method was used to minimise the operator's influence through the positioning pre-processing operations (Appendix B). The method calculated the target position of selected anatomical landmarks, utilising sequential rigid body translations and rotations, relative to the vehicle geometrical constraints (Appendix B, Table B.I , Fig B.1). Using the marionette method [40], positioning simulations were performed to position HBMs and squash seats (Fig B.2 – Fig B.4). The stresses, produced during the positioning stage, were not retained for the HBM but were reinitialised for the seat's foam (using the INITIAL_FOAM_REFERENCE option of LS-DYNA).

The contact force between the IP and the HBM's knees was monitored to determine whether an occupant sitting in the seat adjustment is realistic, with 0.5 kN as the threshold. Occupants with stature above 1617 mm and 1758 mm could not be positioned in the 0% and 20% fore-aft seats, respectively.

The validity of the seat-squashing was controlled by ensuring that the contact force between the occupant and the vehicle interior was approximately equal to the occupant's mass. For all positioning simulations, the contact force between the occupant and the vehicle was within 115–205% (Appendix A, Table A.IV) of the occupant's weight at the end of the positioning (pre)simulations.

The belt was routed to the shortest path over the positioned HBMs, minimising the slack, using the belt routing algorithm of the Primer v17 (Oasys Ltd, Solihull, United Kingdom) software.

Crash Configurations

Four crash configurations were included in this study. Three of the configurations were used in a prior study [22] and described in [41] as representative of potential future intersection crashes. They include two Side impacts – a Near-Side impact to the front right corner and a Far-Side impact to the front left corner – and an (Intersection) Frontal impact with approximately 50% overlap from the left. In addition, a car-to-car frontal crash, with approximately 50% overlap and an initial velocity of 50 kph for both vehicles, was used to represent a high-severity frontal impact, hereafter called Oncoming Frontal.

The crash pulses were generated from car-to-car impact simulations, as described in [22]. The three crash pulses from the intersection crash configurations can be categorised as relatively low-severity impacts, and the Oncoming Frontal as a high-severity impact. The in-crash vehicle motions of the crash simulations are illustrated in Fig. 2.

The HBM in-crash simulations were performed by applying the motion from the car-to-car impacts to the compartment model using prescribed rigid-body six-degrees-of-freedom translational and rotational velocities. The Near-Side and the Frontal impacts were simulated for 200 ms, while the Far-Side was simulated for 300 ms.

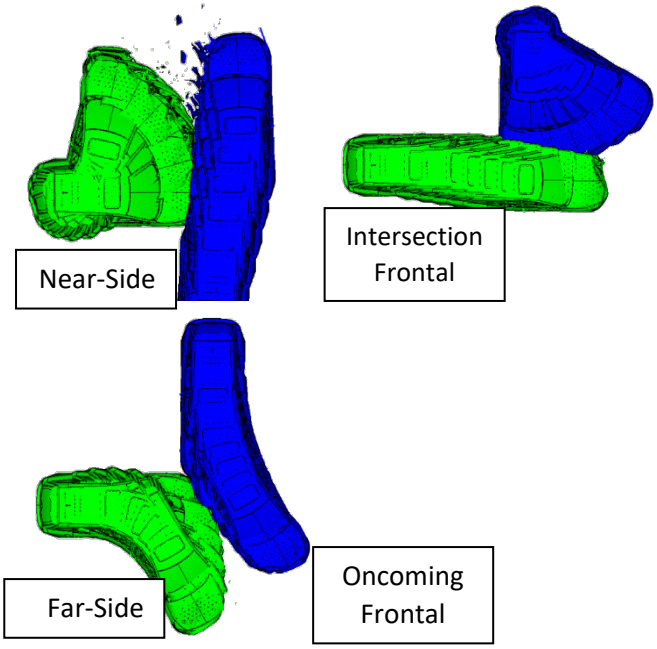

Fig. 2. Vehicle motion of the car-car impact. During the crash simulations, the HBM is located in the front passenger (right) seat of the host vehicle (green).

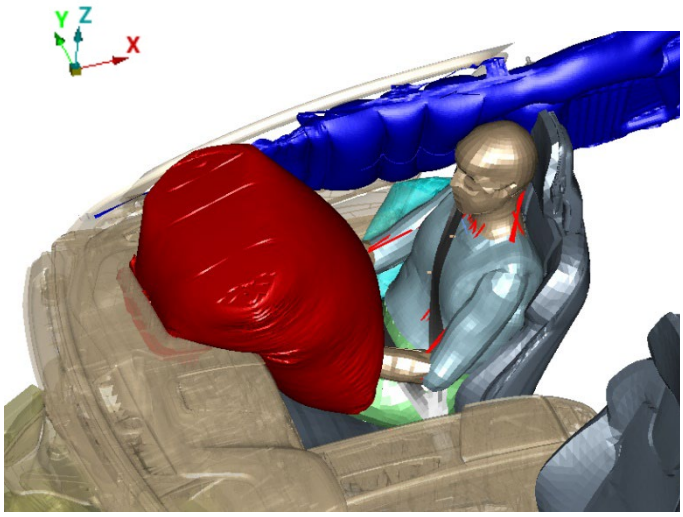

Fig. 3. The vehicle interior model with the baseline HBM and deployed airbags (frontal in red, inflatable curtain in blue, and torso in cyan) is illustrated.

Analysis Methods

The initial belt fit was quantified by measuring the distance of the lap belt relative to the HBM's Anterior Superior Iliac Spine (ASIS), and of the shoulder belt relative to the HBM's sternum (at the sixth rib height) and the acromial end of the clavicle. Furthermore, the presence of submarining, defined as the lap belt sliding over either of the two ASIS, was manually inspected in the frontal impacts.

The occupant responses were compared by analysing occupant kinematics and kinetics. Kinematics included three-dimensional excursions and (X-, Y-, Z-, and resultant) velocities of selected anatomical landmarks relative to the vehicle. Additionally, the pelvic angle [42], torso angle, and the head Frankfurt plane orientation were tracked. The torso angle was defined on the XZ (pitch) and YZ plane using the sacrum and T8 vertebra, while the rotation around the Z-axis was calculated using the left and right acromion. The kinetic responses were analysed by considering loads (X-, Y-, Z-, and resultant forces and moments) at cross-sections of the HBM. The inclusive list of analysed responses can be seen in Appendix C. The analysis was performed in two steps. First, cross-correlation was performed to quantify and rank the parameters' influence per body region. Then, as a second step, Global Sensitivity Analysis (GSA) was performed to identify kinematic and kinetic patterns in all affected body regions.

Global Sensitivity Analysis

A GSA method was developed and applied to investigate the effect of the studied parameters on occupant responses. The elementary effects (EE) method, first introduced by Morris [43], was used as the foundation of the method. The Morris EE method is a one-at-a-time (OAT) analysis, typically used to investigate local variation around a base point when the number of input factors is large [44]. By calculating local variations at different points of the input space, the EE method can be regarded as a GSA [45]. The developed method (Appendix D) includes an alternate sampling strategy, a group-analysis approach, and an updated sensitivity output metric calculation. The occupant responses were grouped following the OAT approach, and the sensitivity metric was calculated by utilising median and interquartile ranges (25^{th} to 75^{th} percentile). Additionally, the Wilcoxon (two-sided) signed rank test, as implemented in MATLAB R2017b (MathWorks, Massachusetts, USA), was performed on the compared groups, with $p \leq 0.05$ as the cut-off, to evaluate the consistency of the identified trends. The updated method can be considered as an extension of the EE method, with the added capabilities of analysing interaction effects as well as reporting the confidence intervals of the effects.

Cross-Correlation Analysis

To systematically quantify the extent of change in occupant responses, cross-correlation was calculated using CORA [46]. The shape and amplitude of the responses were weighted by 0.5, and responses with low magnitude

[22] were excluded from the analysis. Identical responses got a perfect CORA score (1), while largely altered responses got CORA scores close to 0. In order to determine a body region's response cross-correlation, the Root Mean Square (RMS) addition [47] was used to combine the cross-correlation value of all responses belonging to the body region. GSA was applied to the body regions' cross-correlation results to study and rank the effects of the investigated parameters on occupant responses. CORA reduction ($CORA_{reduction}$ = 1-CORA) was used to perform the GSA calculations. The sensitivity analysis considered the most influential level for every parameter, as seen in the example (Appendix E, Fig. E.1). Performing GSA on the CORA considers the whole sequence of the responses.

III. RESULTS

Patterns in the initial occupant's distance to the vehicle interior, posture and belt fit were analysed after the HBM positioning simulations. In general, it was found that fore-aft position and stature affected the distance between the knees and the dashboard (Appendix B, Table B.II). Increasing the BMI positioned the H-Point higher and more forward relative to the seat and altered the belt fit. The lap-belt was higher and more forward relative to the ASIS (Fig. B.5), and the shoulder-belt was more inboard (medially on the clavicle) (Fig. B.6). The backrest angle altered the pelvic and torso pitch angle, as well as the distance between the head and the dashboard. Furthermore, a 7.5° more reclined pelvis was observed for female occupants. More detailed information about the distance to interior, posture and belt fit can be found in Appendix B (Table B.II – Table B.IV).

All 944 simulations reached normal termination regardless of occupant shape and size or seat adjustment. The ratio of hourglass energy to total energy, for the whole model, at the final timestep had a median value of 3.7% for the Oncoming Frontal simulations. BMI was the only parameter influencing the hourglass energy ratio, with a median increase of 2% for obese (38 kg/m^2) occupants and a median reduction of 1.1% for underweight (18 kg/m^2) occupants. A similar trend was seen in the rest of the simulated impacts. However, it was less apparent due to the generally lower hourglass energy ratios.

Ranking of Parameters' Influence – Cross-correlation

The cross-correlation, which was performed to quantify and rank the parameters' influence per body region, resulted in the CORA matrix. The CORA values in every cell represented the maximum median change observed when a parameter was changed. Low numbers (visualised in red) indicate altered responses, while numbers closer to one (visualised in green) indicate unchanged responses. An example of the CORA score calculation can be seen in Appendix E (Fig. E.1). Table I and Table II contains the results for the Intersection Frontal, and Oncoming Frontal impacts, respectively. The results of the Near-Side and Far-Side impacts can be found in Table F.I and Table F.II.

Intersection Frontal

In the Intersection Frontal impact (Table I), the pelvis kinematics were mainly influenced by the fore-aft position (0.78) and BMI (0.64). The spine kinematics were also affected by BMI and the fore-aft position, with the largest effects being seen in the lumbar (0.68, 0.73) and thoracic (0.72, 0.71) regions. The lower extremities kinematics were influenced by the fore-aft position (0.63), BMI (0.65) and stature (0.6). The upper extremities kinematics and kinetics were influenced by all parameters, with the largest deviation being seen when the fore-aft position (0.54, 0.53), the BMI (0.53, 0.47) and stature (0.62, 0.56) were altered.

TABLE I
INTERSECTION FRONTAL CORA RESULTS – ALTERED RESPONSES ARE VISUALISED IN RED

	Kinematics								Kinetics				
	Pelvis	Spine (Lumbar)	Spine (Thoracic)	Spine (Cervical)	Torso	Head	Extremities Lower	Extremities Upper	Pelvis	Spine (Lumbar)	Spine (Cervical)	Extremities Lower	Extremities Upper
Backrest	0.91	0.96	0.91	0.89	0.89	0.88	0.90	0.71	0.83	0.90	0.83	0.84	0.73
Fore-Aft	0.78	0.73	0.71	0.80	0.81	0.80	0.63	0.54	0.67	0.74	0.67	0.42	0.53
BMI	0.64	0.68	0.72	0.70	0.77	0.75	0.65	0.53	0.59	0.75	0.64	0.48	0.47
Stature	0.86	0.92	0.90	0.92	0.88	0.91	0.60	0.62	0.72	0.88	0.80	0.40	0.56
Sex	0.91	0.97	0.96	0.96	0.91	0.90	0.84	0.79	0.69	0.84	0.80	0.71	0.76

Oncoming Frontal

In the Oncoming Frontal impact (Table II), mainly the fore-aft position, BMI and stature influenced the pelvis (0.73, 0.65, 0.8), lumbar spine (0.74, 0.67, 0.72) and thoracic spine (0.69, 0.63, 0.76) kinematics. The cervical spine and head kinematic responses were affected by the fore-aft position (0.69, 0.68) and BMI (0.65, 0.73). Additionally, the fore-aft position (0.56), BMI (0.61) and stature (0.62) were associated with altered kinematics of the lower extremities. The upper extremities motion was particularly affected by the fore-aft position (0.56), BMI (0.53) and stature (0.66). The pelvis loading was largely influenced by BMI (0.49), fore-aft position (0.6), as well as stature (0.66) and sex (0.68). The lumbar and cervical spine kinetics were influenced by the fore-aft position and BMI, with CORA scores of 0.65 and 0.54, respectively. The lower and upper extremities loading was largely affected by the fore-aft position, BMI and stature, with scores between 0.38 and 0.4 and between 0.39 and 0.42, respectively. The sex parameter also influenced the lower and upper extremity kinetics, with scores of 0.67 and 0.62.

TABLE II
ONCOMING FRONTAL CORA RESULTS – ALTERED RESPONSES ARE VISUALISED IN RED

	Kinematics								Kinetics				
	Pelvis	Spine (Lumbar)	Spine (Thoracic)	Spine (Cervical)	Torso	Head	Extremities Lower	Extremities Upper	Pelvis	Spine (Lumbar)	Spine (Cervical)	Extremities Lower	Extremities Upper
Backrest	0.91	0.93	0.88	0.93	0.92	0.91	0.88	0.74	0.79	0.88	0.78	0.81	0.64
Fore-Aft	0.73	0.74	0.69	0.69	0.81	0.68	0.56	0.56	0.60	0.65	0.54	0.38	0.42
BMI	0.65	0.67	0.63	0.65	0.77	0.73	0.61	0.53	0.49	0.65	0.54	0.39	0.39
Stature	0.80	0.72	0.76	0.84	0.84	0.85	0.62	0.66	0.66	0.79	0.61	0.40	0.43
Sex	0.88	0.89	0.91	0.94	0.91	0.91	0.81	0.74	0.68	0.80	0.72	0.67	0.62

Patterns of Peak Kinematic and Kinetic Responses

GSA was performed as a second step of the analysis process to identify patterns in the peak values of both kinetic and kinematic responses in all affected body regions. The analysis of kinematic responses consisted of comparisons of the occupant's peak rotation, excursion and velocities relative to the vehicle. Kinetic responses were analysed by comparing the magnitude of moments and forces in cross-sections of the HBM. The main kinematic and kinetic patterns for the Intersection Frontal, and Oncoming Frontal impacts are presented below, while the main patterns for the Near-Side and Far-Side impacts can be found in Appendix F. The results of the GSA can be found in more detail in Table G.I to Table G.IV in Appendix G, for all crash configurations.

Intersection Frontal

In the Intersection Frontal impact simulation, reclining the backrest angle to 30° increased the peak torso resultant speed by 11%. The seat's fore-aft position influenced the pelvis kinematics, with 9% more pelvis excursion and 8° higher pelvis rotation. Interaction effects were seen between peak pelvic Y-angle and stature and BMI. The pelvis of occupants with a BMI of 18 kg/m^2 rotated 14° more when seated in the most rearward position, compared to occupants with nominal BMI in the nominal fore-aft position. Similarly, the pelvis of occupants with stature 1476 mm and 1617 rotated 12° more. The opposite effect was observed when the seat was in the most forward position with reduced pelvis Y rotations of 2°. In parallel to the increased excursions, increased ASIS force was observed (0.2 kN, +20%) in the most rearward position. Additionally, occupants in the most rearward position reached 0.4 m/s (+16%) higher torso and head (0.5 m/s, +9%) speed relative to the vehicle interior. No consistent association between femur forces and fore-aft position was found, due to the existence of interaction effects between BMI, stature and fore-aft position; occupants with high BMI demonstrated increased (up to 1.2 kN) femur forces in the most forward position (which explains the reduced pelvis loading), while the femur force was reduced for occupants with BMI below 28 kg/m^2. Similarly, the femur force of tall (1899 mm)

occupants was reduced (-1.1 kN) in the most rearward position, while it was increased up to 0.5 kN for occupants with stature below 1758 mm. Despite that, the tibia forces were consistently increased up to 77% in the most forward position and reduced up to 45% in the most rearward position.

BMI was associated with increased pelvis X-excursions; however, no consistent association between BMI and peak pelvic angle was seen in the simulations. Obese occupants reached a higher (0.2 m/s) peak torso relative speed, while underweight occupants showed 0.1 m/s reduced peak torso relative speed. A U-shape response was seen between BMI and torso Z-rotation for male occupants, with 8° higher rotations for obese and underweight occupants. Obese female occupants showed a similar trend, but underweight females rotated 2° less than nominal BMI female occupants.

Stature was linked to altered pelvis kinematics. Up to 4.5° of increased pelvic Y-rotation was found by increasing the occupant's stature in steps of 141 mm. However, that trend was not valid for short females with a stature of 1476 mm, compared to nominal height (1617 mm) females, whose pelvis rotated 2° more. Overall, increased lower extremity loads were seen for taller occupants, with up to 0.33 kN higher force and 8 Nm higher moment, per 141 mm of increased stature.

In general, the pelvis kinematic response of female occupants was altered, with 7.5° higher pelvic rotation being observed. However, it should be noted that the initial pelvis orientation was also 7.5° more reclined.

Oncoming Frontal

Reclining the backrest to 30° increased the peak pelvis Y rotation by 4.5°, which was approximately the same as the change of the initial pelvic angle. The lumbar force was increased in the L1 level by 0.4 kN (16%) and the lower neck force by 0.24 kN (16%) when the backrest was reclined.

As with the Intersection Frontal impact simulation, the fore-aft position was highly influential for the pelvis kinematics and kinetics. The maximum longitudinal excursion of the pelvis was increased by 30 mm (Fig. 4), and the pelvis rotated 7° more when the occupant was in the most rearward position. That was more pronounced for underweight occupants, who rotated 19° more, and for short females (1476 mm), who rotated 15° more compared to occupants in the nominal fore-aft position. The pelvic, lumbar and cervical spine loading were increased in the most rearward position. The peak lumbar force at the L1-vertebra was increased by 1.46 kN (+77%) when the seat was in the most rearward position. The opposite effect was seen when adjusting the seat in the most forward position, which reduced the pelvis rotation by 8° and excursion by 25 mm (Fig. 4), as well as the pelvic and spinal loading. On the other hand, adjusting the seat to the most forward position resulted in increased loading of the lower extremities. The left lower tibia magnitude of force was increased by 1 kN. Occupants with high BMI (38 kg/m^2) were associated with up to 1.5 kN increased left femur force and 1.1 kN increased right femur force when in the full-forward position.

BMI was the most influential parameter for the pelvis X-excursions, with underweight occupants moving 72 mm less and obese occupants moving 23 mm more than nominal BMI occupants (Fig. 4). It should be noted that interaction effects between BMI and fore-aft position were present. The influence of BMI was reduced when the seat was adjusted between the most forward (0%) and mid fore-aft (40%) positions (Fig. 4). Because of the interaction between the occupant's knees and the IP, the increased pelvis X-excursions for obese occupants were limited (Fig. 5).

A U-shape relation was observed between BMI and peak pelvic Y angle, with 5.6° and 7.8° higher rotations noticed for obese and underweight occupants, respectively (Fig. 6). Male occupants were affected by low BMI (+10°), while females were not affected (Fig. 6). Interaction effects were also seen between fore-aft position and BMI. Underweight occupants were not consistent with the general findings when positioned in the full forward position, with up to 12° less pelvis rotation compared to occupants of nominal BMI (Fig. 6). A reverse U-shape relation was observed between BMI and kinetics of the pelvic and lumbar spine region, with underweight and overweight occupants being generally exposed to larger pelvis loads compared to occupants of nominal BMI. Obese occupants reached a higher (0.45 m/s, 7%) peak torso relative speed, while underweight occupants reached 0.75 m/s (-11%) lower speed. A minor influence (±0.15 m/s) of BMI on head speed was seen. However, the head rotations were considerably altered by BMI. Underweight occupants showed increased (+25°) head rotations around the Z-axis, and overweight occupants showed decreased (-31°) rotations compared to occupants with nominal BMI. In contrast to that, a U-shape response was seen between lower neck loading and BMI, with

occupants of non-nominal BMI being subjected to higher (0.2 kN, 14%) forces. Additionally, obese occupants were subjected to higher loading in the lower extremities.

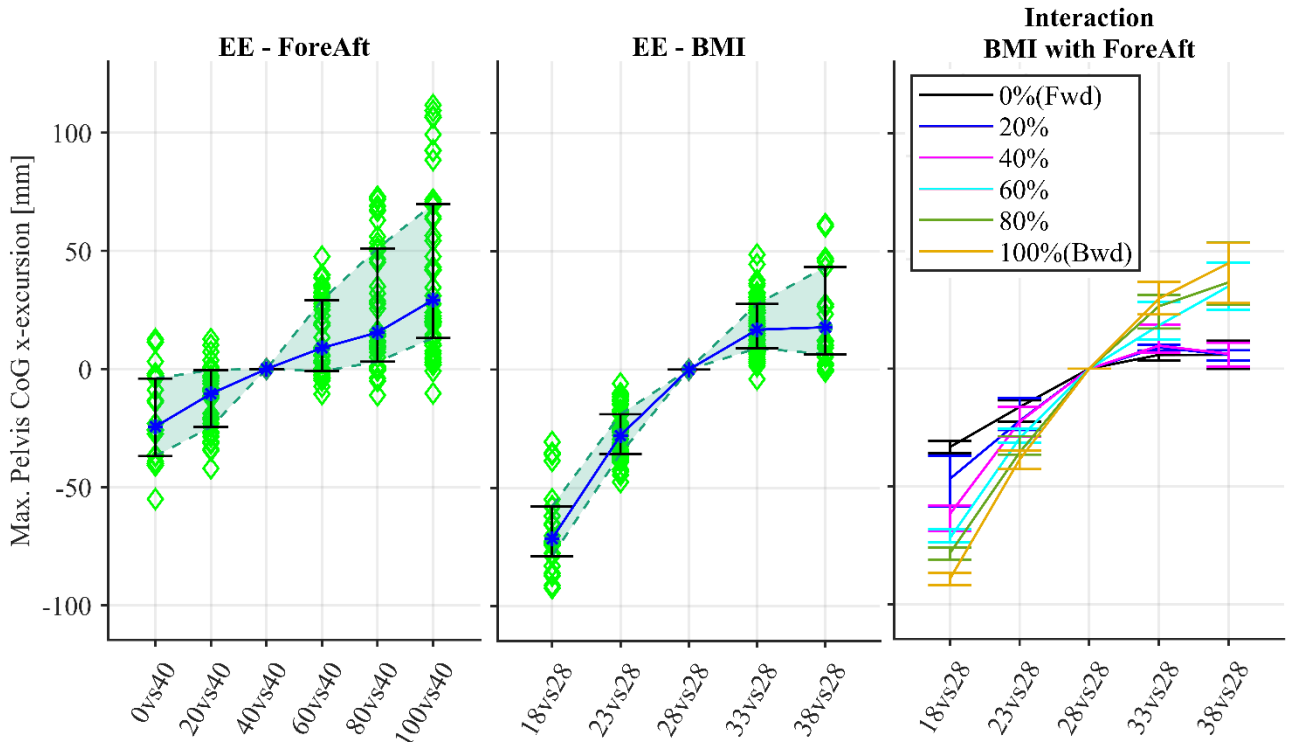

Fig. 4. Influence of BMI and fore-aft position on the maximum pelvis X-excursion in the Oncoming impact simulations. In general, obese or rearwards positioned occupants experienced increased pelvis longitudinal excursions. In contrast, underweight or forward positioned occupants moved less than occupants with nominal BMI or in the nominal fore-aft position. Additionally, interaction effects between BMI and fore-aft position were also seen. The pelvis of obese occupants moved approx. 7mm more compared to occupants of nominal BMI when they were in the 0%,20%, and 40% fore-aft positions. However, their pelvis moved up to 45mm more when positioned in the most rearwards position.

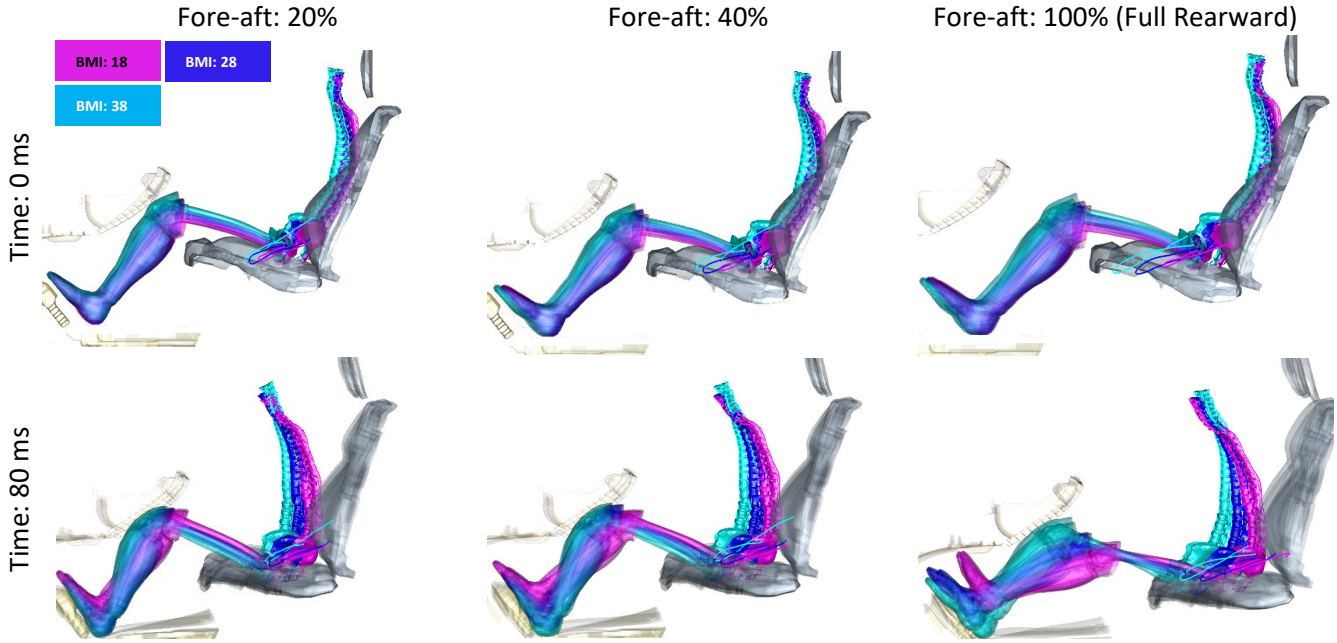

Fig. 5. BMI influence on maximum pelvis excursion, in three fore-aft adjustments; initial (top) and maximum excursion (bottom) timesteps. Obese (cyan) occupants were in general associated with increased longitudinal pelvis excursions in the Oncoming Frontal impact. The influence of BMI is magnified by moving the seat rearward and increased when moving the seat forward, due to the contact between the knees and the IP.

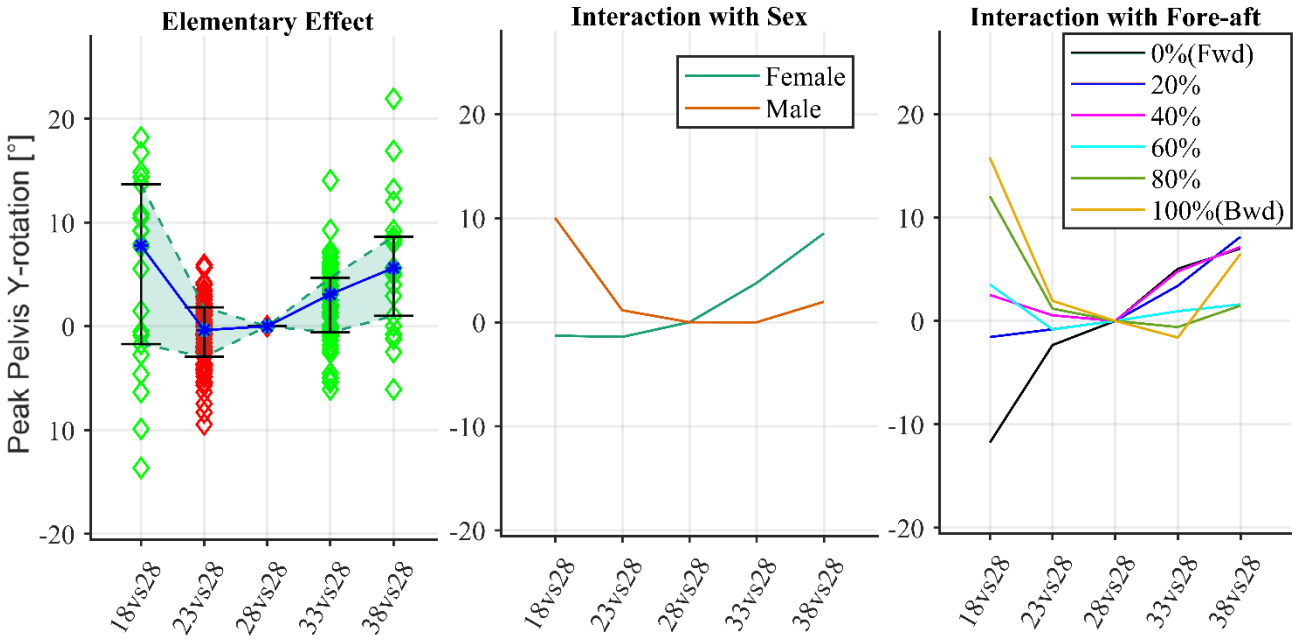

Fig. 6. The influence of BMI on peak pelvis Y-angle during the Oncoming impact simulations is illustrated. Increasing or reducing the BMI from the nominal (28 kg/m^2) resulted in increased pelvic rotation, which resulted in a U-shaped response. Interaction effects were observed between sex and fore-aft position and BMI. Those interaction effects increased the Interquartile Range (IQR), seen with green area, and resulted in inconsistent trends for the 23 vs. 28 kg/m^2 comparison (red markers). Underweight male occupants reached a higher peak pelvic angle, while the opposite trend was seen for underweight female occupants. Additionally, the fore-aft position was influential in the pelvic rotation of underweight occupants. Positioning underweight occupants more forward reduced their peak pelvic rotation, while the opposite effect was seen in more rearward positions.

Submarining was observed in approximately 10% of the Oncoming Frontal simulations, predominantly associated with reclined short female HBMs. It occurred just prior to the pelvis rebound and had minor effect on the HBM kinematics. Stature substantially affected the pelvis rotation, with taller occupants reaching up to 9° higher peak rotation per 141 mm of stature increase. Females were generally more sensitive to stature than male occupants. The lower extremities loading was increased when the stature was increased, while, simultaneously, a reduction in the pelvic loading was observed, indicating a change in the occupant load path in the model.

Increased pelvic loads were measured for female occupants compared to males, and the peak torso speed was reduced by 0.3 m/s (-4%) compared to males of the same stature and BMI. The lumbar force at the L5 level was increased by 0.3 kN (25%), while the lower neck force was reduced by 0.25 kN (-18%) and the lower neck moment by 35 Nm (-33%).

IV. DISCUSSION

The influence of occupant anthropometry and seat adjustment on occupant kinematics and kinetics in impacts was investigated in a numerical simulation study. As seen in previous studies [3-5], variations in occupant anthropometry led to altered occupant responses, with complex interaction effects between the anthropometric parameters. Compared to past studies, the sensitivity analysis in this study utilised one-at-a-time parameter perturbations at a multitude of input space points, which enabled ascribing the observed responses to a single parameter change, allowed interactions effects to be studied and provided multiple observations across the parameter space. In addition, multiple crash configurations were included in the current study, ranging from low-severity intersection to high-severity oncoming impacts, providing a more complete understanding in relation to the diverse impacts that could occur in real-world traffic.

Among the main findings of this study was the identification of BMI as the most influential parameter for pelvis kinematics and kinetic responses across all evaluated crash configurations. The forces and moments measured in the lower and upper extremity regions of the HBM were generally higher as the stature and the BMI of the occupant increased. BMI was also associated with altered head kinematics and cervical spine loading. The load increase found across most body regions when BMI was increased could potentially contribute to the increased

injury rate for occupants with high BMI seen in field studies [1-5].

In Frontal impacts, the present study described altered kinetics of the cervical spine, with up to 106% increased cervical spine moment for obese occupants, which stands in contrast to Hu *et al.* [10], who could not identify parameters influencing the cervical spine response. Furthermore, BMI, stature and fore-aft position of the seat were very influential for the lower and upper extremities' kinematic and kinetic responses. In the Oncoming Frontal simulations, increased lower extremities loading was seen with a median increase of femur force of 0.8 kN for obese occupants (38 vs. 28 kg/m^2). Similarly, Shi *et al.* [48] reported an increase of 1.5 kN of femur force for obese occupants (40 vs. 25 kg/m^2). In the current study, besides increased loading for the femur, higher forces were consistently measured in the tibia when the BMI or stature were increased or when the seat was positioned more forward. Additionally, increased pelvis excursions were identified for obese occupants, as also seen in [15]. The influence of BMI on maximum pelvis excursions was exaggerated when the seat was moved rearwards and reduced when the seat was moved forward; implying that the knee restraint could be more important for obese occupants. Moreover, in contrast to [15], no consistent change in torso pitch angle was observed for obese occupants. This difference could be an effect of the different vehicle environments used; here, a front passenger environment was used compared to the rear-seat environment used by Kent *et al*. [15]. Furthermore, increased maximum pelvis rotation was observed not only for obese but also for underweight occupants (Fig. 6).

Past studies have identified increased lumbar spine loading for reclined postures [19][49]. In the present study it was found that in the high-severity Oncoming Frontal impact simulations, positioning the seat in the most-rearward position could lead to a larger increase in lumbar spine loading than semi-reclining the backrest. Therefore, investigating further the possible effects of knee restraints, in regards not only to lower extremities but also to pelvic and spinal loading, could be beneficial. Positioning the seat more forward resulted generally in higher lower extremities loads, which could result in increased lower extremities injury risk, as also seen for drivers [17]. Those results indicate that there might be a trade-off not only between lumbar forces and submarining risk when reclining [49] but also between lower extremities and lumbar spine loading when adjusting the fore-aft position.

Adjusting the seat position rearwards led to increased head relative speed in the Frontal impacts, while the opposite trend was seen in the Side impacts (see Appendix F). While the first observation was not surprising due to the altered distance of the occupant with the vehicle interior, the second was unexpected. The mechanism behind the increased velocities observed in the Side impacts is likely the rotational motion of the vehicle induced by impacts in the vehicle's front corners, which are expected to be more frequent in future intersection crashes [41][50]. Moving the occupants forward is also moving them away from the rotation centre of the vehicle, increasing their relative speed. Sitting more forward than the mid-travel is expected to be infrequent [16]. Despite that, sitting more forward is possible and might be necessary in some cases (for example, in the presence of tall rear-seat occupants) and is, therefore, an interesting finding.

Differences in the pelvis, as well as spine, kinematic and kinetic responses, were also seen between male and female occupants of identical stature and body mass. Those differences originated from the altered soft-tissue distribution, which resulted in different initial belt fit and posture during the positioning phase. The applied positioning method predicted females to have more (7.5°) reclined pelvis compared to males of the same stature and BMI. This was partly due to the altered adipose tissue distribution and its interaction with the seat, as well as due to the less pronounced ASIS, which altered the pelvic angle measurement [42] comparability. This change was comparable with [23], which predicted an 8.9° more reclined pelvis for a female compared to a male, with a stature of 1617 mm and BMI of 28 kg/m^2. The data for [23] were insufficient for comparing males and females beyond that stature and BMI. A similar trend, although smaller in magnitude, was seen in [42], in which seated females had an average pelvic angle 2.5° more reclined compared to seated males. Additionally, it should be noted that the standard deviation of the pelvic angle for occupants in automotive seat was in the range of 10° [42] and the positioned models were within one standard deviation. In the Frontal impact simulations, the analysis for female occupants identified similar patterns between male to female and upright to semi-reclined occupants. That was probably because when semi-reclining by 5°, the initial pelvic angle was similarly affected as comparing females and males. Therefore, further studies investigating sex-related differences in the initial pelvic angle would be beneficial. Regarding the increased injury ratios found for female compared to male occupants in field studies [6], it should also be considered that the median stature of female and male occupants is different. In this study, comparing the response of occupants with a stature of 1476 mm (only female models) with

occupants of stature 1617mm was more influential than comparing females and males of the same stature. Some of the differences in the field could therefore be linked to the different stature distribution.

In this study, the sex-related body shape differences, such as adipose tissue distribution and altered centre of gravity, were investigated. To perform a comparison between males and females regarding injury risk, more parameters should be included, such as material and structural property variations of individual bones [51-53] or soft-tissue. Those aspects could influence the injury tolerance between females and males. Besides anatomical variation between males and females, large variation across individuals exists. For this study, HBMs were generated to represent the average anthropometric target of a given BMI, stature, age and sex. HBMs representing average anthropometries have been as good as subject-specific HBMs in predicting kinematics [34]. However, individual injury tolerance could be important to consider when performing injury predictions. Scaling techniques that try to account for occupant variability exist [54] and are frequently used to normalise responses and generate corridors from biological experiments. Those techniques could be used to consider the effects of covariate factors, such as occupant's stature, that could influence injury tolerance. However, those techniques were not used in the present study as they typically generate too-wide corridors, failing to explain injury variability based on anthropometric properties [54]. As also discussed in [10], when "simple" methods (such as mass-scaling) were applied to parametric HBM results, they could not appropriately account for variations due to occupant shape and were therefore considered inadequate for capturing the altered injury tolerance. Additionally, it was found that the general injury trends were consistent regardless of using or not using scaling techniques [10]. Tissue-level injury prediction could be beneficial for capturing those effects. However, in their current state, further development is needed [34][37] to validate the injury prediction capabilities of morphed HBMs. Additionally, due to the potential presence of altered injury tolerance, the lack of kinetic trends could still be associated with higher or lower injury risk for certain anthropometries. For example, if no change in lumbar compression forces is seen between short and nominal stature occupants, that could be an indication that shorter occupants are at a higher risk, as shorter occupants most likely have smaller vertebras, potentially tolerating a smaller force.

The use of FE models allowed for a controlled environment, enabling the OAT approach adopted in this study. This approach was straightforward for analysing elementary and interaction effects. However, it was computationally expensive, therefore the number of investigated parameters had to be limited. That was among the motivations for not investigating the effect of age, alongside the fact that age would not only alter the body shape but could also alter the posture [23] and the injury tolerance substantially. Additionally, past studies [8] have identified age as an important parameter to be considered, as elderly occupants were found to be at increased risk. A computational study [12] investigated the effect of age-related shape differences and led to unexpected results, such as stiffer thorax with higher peak force and lower chest deflection. To fully understand the effects of age, the material properties in these models need to be also considered. HBMs are ideal tools for investigating the effects of those parameters. However, at the time this study was performed, the used HBM did not have those capabilities.

The range of the chosen input parameter space is crucial when performing GSA [55]. Therefore, in this study, statistical analysis was performed to determine the BMI and stature combinations that included approximately 90% of the US population. Nonetheless, modelling limitations needed to be taken into account, therefore no occupants with BMI below 18 kg/m^2 or above 38 kg/m^2 were simulated, as achieving acceptable model element quality for those occupants would have been challenging. Additionally, the backrest angle was reclined only up to 30°. Reclining it further could potentially increase its influence on the occupant response.

The two analysis steps are complementary to each other. The cross-correlation carried out considered the entire sequence of kinematic and kinetic responses, while the second step provided numbers that were easy to comprehend and relate to potential occupant injury risk. In the second part of the analysis in this study, the magnitude of loads (forces and moment) was used to give some insights into the kinetic trends while reducing the amount of the reported responses. In some cases, however, different loading mechanisms can be masked when analysing the magnitude of loads. In the Oncoming Frontal impacts, for example, tall occupants (1899 mm) were subjected to reduced femur force when the seat was moved rearwards, in contrast to shorter occupants (below 1756 mm) who were subjected to reduced femur force when the seat was moved forward. Despite the "similar" recorded effect, there were two different mechanisms behind those trends leading to different loading of the femurs. Taller occupants offloaded the compressive forces in rearward positions, while shorter occupants

got less tensile force in the forward positions. Therefore, identifying the loading mechanisms for the highlighted influential parameters is subject to future studies.

No variation of sitting posture was included for the combination of occupant size and seat position. However, occupants can be out of the nominal position, which can influence their kinematic and kinetic response [22]. The influence of non-nominal postures could be exaggerated in the presence of diverse anthropometry or altered seat adjustment. Similarly, in the real-world, variations could also exist in the occupant belt fit. In this study, the belt was routed following the shortest path and the belt fit patterns observed related to BMI were comparable with the trends reported in the laboratory study [21], but the sex effects were not in agreement (the lap-belt was 24 mm more forward in [21], and 4 mm less forward for men in the present study). Additionally, the belt fit could be influenced considerably by parameters beyond BMI, stature and sex [21], such as choice of clothes or occupant's individual body shape, posture and comfort perception.

This study highlights occupant protection challenges, using HBM simulations, and can be used to further enhance occupant protection, considering occupant anthropometric diversity and seat adjustment variation. Future work to address the limitations presented earlier, such as the lack of tissue-level injury prediction functionality and understanding of individual anthropometric variability and injury tolerance, can further enhance the population coverage of morphed HBMs, leading to more inclusive occupant safety assessment.

V. CONCLUSIONS

The developed GSA method quantified the primary and interaction effects and, by utilising statistical testing, could highlight the consistency of the observed trends in the simulations of a diverse family of occupants seated in a multitude of seat adjustments. Across all evaluated crash configurations simulated, increased pelvis excursion and loading were observed for occupants with increased BMI. In addition, BMI also influenced the head kinematics and cervical spine loading. The forces and moments measured in the lower and upper extremity regions were generally higher as the stature and the BMI of the occupant increased. Adjusting the fore-aft position of the seat was very influential for the extremities' kinematics and kinetics. In Frontal impact simulations, reclining the occupant was associated with increased lumbar spine loading. However, adjusting the seat's fore-aft position had a larger influence on the lumbar loading. Furthermore, a trade-off between pelvis/lumbar spine loading and lower extremities was seen when adjusting the fore-aft position of the seat. The increased lower extremities forces measured in the most forward position were accompanied by reduced pelvic and lumbar spine loading, while positioning the HBM more rearward reduced the lower extremity forces but increased the lumbar spine loading. Additionally, a trend of larger pelvis rotations in the Oncoming Frontal impact was seen for occupants with non-nominal BMI. In the Side impacts, moving the seat in the most forward position increased the torso and head speed relative to the vehicle. Protection of extremities and lumbar spine could benefit by including occupants with increased stature, non-nominal BMI, as well as rearward positioned seats in the safety evaluations.

VI. ACKNOWLEDGEMENTS

The work was carried out at SAFER Vehicle and Traffic Safety Centre at Chalmers as part of The European Union Horizon 2020 Research and Innovation programme project, VIRTUAL. VIRTUAL has received funding from the European Union's Horizon 2020 research and innovation programme under grant agreement No 768960.

The authors are grateful to Karl-Johan Larsson for his valuable support in the HBM morphing process and for all the constructive discussions. Additionally, the authors would like to thank the participants of VIRTUAL WP2 and WP3 for the fruitful discussions during the project meetings. The content of this publication does not reflect the official opinion of the European Union. Responsibility for the information and views expressed therein lies entirely with the authors.

VII. REFERENCES

[1] Viano, D. C., Parenteau, C. S., Edwards, M. L. (2008) Crash Injury Risks for Obese Occupants Using a Matched-Pair Analysis. *Traffic Injury Prevention*, **9**(1): pp.59–64, doi:10.1080/15389580701737645.

[2] Joodaki, H., Gepner, B., McMurry, T, Kerrigan, J. (2020) Comparison of injuries of belted occupants among different BMI categories in frontal crashes. *International Journal of Obesity*, **44**(6): pp.1319–1329, doi:10.1038/s41366-019-0481-2.

[3] Rupp, J. D., Flannagan, C. A. C., *et al.* (2013) Effects of BMI on the risk and frequency of AIS 3+ injuries in motor-vehicle crashes. *Obesity*, **21**(1): pp.E88–E97. doi:10.1002/oby.20079.
[4] Forman, J. L., McMurry, T. L. (2018) Nonlinear models of injury risk and implications in intervention targeting for thoracic injury mitigation. *Traffic Injury Prevention*, **19**(sup2): pp.S103–S108. doi:10.1080/15389588.2018.1528356.
[5] Zhu, S., Kim, J. E., *et al.* (2010) BMI and risk of serious upper body injury following motor vehicle crashes: Concordance of real-world and computer-simulated observations. *PLoS Medicine*, **7**(3): pp.1–13. doi:10.1371/journal.pmed.1000250.
[6] Forman, J., Poplin, G. S., *et al.* (2019) Automobile injury trends in the contemporary fleet: Belted occupants in frontal collisions. *Traffic Injury Prevention*, **20**(6). doi:10.1080/15389588.2019.1630825.
[7] Yoganandan, N., Arun, M. W. J., *et al*. (2014) Crash Characteristics and Injury Patterns of Restrained Front Seat Occupants in Far-side Impacts. *Traffic Injury Prevention*, **15**(sup1): pp.S27–S34. doi:10.1080/15389588.2014.935771.
[8] Carter, P. M., Flannagan, C. A. C., *et al.* (2014) Comparing the effects of age, BMI and gender on severe injury (AIS 3+) in motor-vehicle crashes. *Accident Analysis and Prevention*, **72**: pp.146–160. doi:10.1016/j.aap.2014.05.024.
[9] Hwang, E., Hu, J., *et al.* (2016) Development, Evaluation, and Sensitivity Analysis of Parametric Finite Element Whole-Body Human Models in Side Impacts. *Stapp Car Crash Journal*, **60**: pp.473–508. PMID: 27871104.
[10] Hu, J., Zhang, K., *et al*. (2019) Frontal crash simulations using parametric human models representing a diverse population. *Traffic Injury Prevention*, **20**(sup1): pp.S97–S105. doi:10.1080/15389588.2019.1581926.
[11] Hu, J., Fanta, A., Neal, M. O., Reed, M. P., Wang, J. T. (2016) Vehicle crash simulations with morphed GHBMC human models of different stature, BMI, and age. Proceedings of the 4th International Digital Human Modeling Symposium (DHM2016), Montréal, Québec, Canada.
[12] Hu, J., Zhang, K., Fanta, A., Hwang, E., Reed, M. P. (2017) Effects of Male Stature and Body Shape on Thoracic Impact Response Using Parametric Finite Element Human Modeling. *Proceedings of the 25th International Technical Conference on the Enhanced Safety of Vehicles (ESV)*, 2017. Paper Number 17-0314.
[13] Hu, J., Zhang, K., *et al.* (2017) Stature and body shape effects on driver injury risks in frontal crashes: A parametric human modelling study. *Proceedings of the IRCOBI Conference*, Antwerp, Belgium: pp.656–667. IRC-17-85.
[14] Boyle, K., Fanta, A., *et al.* (2020) Restraint systems considering occupant diversity and pre-crash posture. *Traffic Injury Prevention*, **21**(sup1): pp.S31–S36. doi:10.1080/15389588.2021.1895989.
[15] Kent, R. W., Forman, J. L., Bostrom, O. (2010) Is there really a “cushion effect”: a biomechanical investigation of crash injury mechanisms in the obese. *Obesity* (Silver Spring), **18**(4): pp.749–753. doi:10.1038/oby.2009.315.
[16] Reed, M. P., Ebert, S. M., Jones, M. L. H., Hallman, J. J. (2020) Prevalence of non-nominal seat positions and postures among front-seat passengers. *Traffic Injury Prevention*, **21**(sup1): pp.S7–S12. doi:10.1080/15389588.2020.1793971.
[17] Hu, J., Rupp, J., *et al.* (2010) Computational investigation of the effects of driver and vehicle interior factors on the risk of knee-thigh-hip injuries in frontal crashes. SAE Technical Paper 2010-01-1023. doi:10.4271/2010-01-1023.
[18] Rawska, K., Gepner, B., *et al.* (2019) Submarining sensitivity across varied anthropometry in an autonomous driving system environment. *Traffic Injury Prevention*, **20**(sup2): pp.S123–S127. doi:10.1080/15389588.2019.1655734.
[19] Boyle, K. J., Reed, M. P., Zaseck, L. W., Hu, J. (2019) A human modelling study on occupant kinematics in highly reclined seats during frontal crashes. *Proceedings of the IRCOBI Conference*, Florence, Italy: pp.282–292. IRC-19-43.
[20] Jones, M. L. H., Ebert, S. M., Hu, J., Reed, M. P. (2017) Effects of high levels of obesity on lap and shoulder belt paths. *Proceedings of the IRCOBI Conference*, Antwerp, Belgium: pp.317–326. IRC-17-50
[21] Jones, M. L. H., Ebert, S. M., *et al.* (2021) Effect of Class I–III obesity on driver seat belt fit. *Traffic Injury Prevention*, **22**(7): pp.547–552. doi:10.1080/15389588.2021.1945590.
[22] Leledakis, A., Östh, J., Davidsson, J., Jakobsson, L. (2021) The influence of car passengers’ sitting postures in intersection crashes. *Accident Analysis & Prevention*, **157**. doi:10.1016/j.aap.2021.106170.
[23] Park, J., Ebert, S. M., Reed, M. P., Hallman, J. J. (2016) A statistical model including age to predict passenger postures in the rear seats of automobiles. *Ergonomics*, **59**(6): pp.796–805. doi:10.1080/00140139.2015.1088076.

[24] Perez-Rapela, D., Forman, J. L., Huddleston, S. H., Crandall, J. R. (2020) Methodology for vehicle safety development and assessment accounting for occupant response variability to human and non-human factors. *Computer Methods in Biomechanics and Biomedical Engineering*, **24**(4): pp.384–399. doi:10.1080/10255842.2020.1830380.

[25] Joodaki, H., Gepner, B., Kerrigan, J. (2021) Leveraging machine learning for predicting human body model response in restraint design simulations. *Computer Methods in Biomechanics and Biomedical Engineering*, **24**(6): pp.597–611. doi:10.1080/10255842.2020.1841754.

[26] Joodaki, H., Gepner, B., , S. H., Katagiri, M., Kim, T., Kerrigan, J. (2021) Is optimized restraint system for an occupant with obesity different than that for a normal BMI occupant? *Traffic Injury Prevention*, **22**(8): pp.623–628. doi:10.1080/15389588.2021.1965131.

[27] Centers for Disease Control and Prevention/National Center for Health Statistics (2018) National Health and Nutrition Examination Survey: Analytic Guidelines, 2011-2014 and 2015-2016. Available at: https://wwwn.cdc.gov/nchs/data/nhanes/analyticguidelines/11-16-analytic-guidelines.pdf. [Accessed: 21 March 2022]

[28] Courant, R., Robbins, H. (1996) What is mathematics?: an elementary approach to ideas and methods. Oxford University Press, Oxford, England: p.343.

[29] National Highway Traffic Safety Administration (2019) National Automotive Sampling System (NASS) General Estimates System (GES); Analytical User's Manual 1988–2015. DOT HS 812 320.

[30] World Health Organization (WHO) (2005) The Surveillance of Risk Factors (SuRF) Report 2. Geneva, Switzerland, 2005. ISBN 92 4 159302 4.

[31] Östh, J., Bohman, K., Jakobsson, L. (2020) Evaluation of Kinematics and Restraint Interaction when Repositioning a Driver from a Reclined to an Upright Position Prior to Frontal Impact using Active Human Body Model Simulations. *Proceedings of the IRCOBI Conference*, Online, 2020: pp.358–380. IRC-20-50.

[32] Pipkorn, B., Iraeus, J., Björklund, M., Bunketorp, O., Jakobsson, L. (2019) Multi-scale validation of a rib fracture prediction method for human body models. *Proceedings of the IRCOBI Conference*, Florence, Italy: pp.175–192. IRC-19-34.

[33] Iraeus, J., Pipkorn, B. (2019) Development and validation of a generic finite element ribcage to be used for strain-based fracture prediction. *Proceedings of the IRCOBI Conference*, Florence, Italy: pp.193–210. IRC-19-35.

[34] Larsson, K. J., Pipkorn, B., *et al.* (2019) Evaluation of the benefits of parametric human body model morphing for prediction of injury to elderly occupants in side impact. *Proceedings of the IRCOBI Conference*, Florence, Italy: pp.150–174. IRC-19-33.

[35] Mroz, K., Östling, M., *et al.* (2020) Effect of Seat and Seat Belt characteristics on the Lumbar Spine and Pelvis Loading of the SAFER Human Body Model in reclined Postures. *Proceedings of the IRCOBI Conference*, Online: pp.470–486. IRC-20-58.

[36] Pipkorn, B., Larsson, K. J., *et al.* (2018) Occupant protection in far-side impacts. *Proceedings of the IRCOBI Conference*, Athens, Greece: pp.76–105. IRC-18-16.

[37] Hwang, E., Hallman, J., *et al*. (2016) Rapid Development of Diverse Human Body Models for Crash Simulations through Mesh Morphing. SAE Technical Paper 2016-01-1491. doi:10.4271/2016-01-1491.

[38] Larsson, K. J., Pipkorn, B., Iraeus, J., Forman, J., Hu, J. (2021) Evaluation of a diverse population of morphed human body models for prediction of vehicle occupant crash kinematics. *Computer Methods in Biomechanics and Biomedical Engineering*. doi:10.1080/10255842.2021.2003790.

[39] Östh, J., Pipkorn, B., Forsberg, J., Iraeus, J. (2021) Numerical Reproducibility of Human Body Model Crash Simulations. *Proceedings of the IRCOBI Conference*, online: pp.431–441. IRC-21-51.

[40] Poulard, D., Subit, D., Donlon, J-P., Kent, R. W. (2015) Development of a computational framework to adjust the pre-impact spine posture of a whole-body model based on cadaver tests data. *Journal of Biomechanics*, **48**(4): pp.636–643. doi:10.1016/j.jbiomech.2014.12.050.

[41] Leledakis, A., Lindman, M., *et al.* (2021) A method for predicting crash configurations using counterfactual simulations and real-world data. *Accident Analysis & Prevention*, **150**. doi:10.1016/j.aap.2020.105932.

[42] Izumiyama, T., Nishida, N., *et al.* (2018) The analysis of an individual difference in human skeletal alignment in seated posture and occupant behavior using HBMs. *Proceedings of the IRCOBI Conference*, Athens, Greece: pp.549–560. IRC-18-84.

[43] Morris, M. D. (1991) Factorial Sampling Plans for Preliminary Computational Experiments. *Quality Engineering*, **37**: pp.307–310. doi:10.2307/1269043.

[44] Saltelli, A., Ratto, M., *et al.* (2007) Global Sensitivity Analysis. The Primer. Chichester, UK: John Wiley & Sons, Ltd. doi:10.1002/9780470725184.

[45] Campolongo, F., Cariboni, J., Wim, S. (2005) Enhancing the Morris Method. *Proceedings of the Sensitivity Analysis of Model Output* (SAMO): pp.369–379. JRC31319.

[46] Gehre, C., Stahlschmidt, S. (2011) Assessment of dummy models by using objective rating methods. *Proceedings of the 22nd International Technical Conference on the Enhanced Safety of Vehicles* (ESV), Paper Number 11-0216.

[47] Hovenga, P. E., Spit, H. H., Uijldert, M., Dalenoort, A. M. (2005) Improved prediction of hybrid-iii injury values using advanced multibody techniques and objective rating. SAE Technical Paper 2005-01-1307. https://doi.org/10.4271/2005-01-1307.

[48] Shi, X., Cao, L., Reed, M. P., Rupp, J. D., Hu, J. (2015) Effects of obesity on occupant responses in frontal crashes: a simulation analysis using human body models. *Computer Methods in Biomechanics and Biomedical Engineering*, **18**(12): pp.1280–1292. doi:10.1080/10255842.2014.900544.

[49] Tang, L., Zheng, J., Hu, J. (2020) A numerical investigation of factors affecting lumbar spine injuries in frontal crashes. *Accident Analysis & Prevention*, **136**. doi:10.1016/j.aap.2019.105400.

[50] Östling, M., Jeppsson, H., Lubbe, N. (2019) Predicting crash configurations in passenger car to passenger car crashes to guide the development of future passenger car safety. *Proceedings of the IRCOBI Conference*, Florence, Italy: pp.626–643. IRC-19-92.

[51] Schubert, A., Erlinger, N., *et al*. (2021) Development of a 50th Percentile Female Femur Model. *Proceedings of the IRCOBI Conference*, online: pp.308–332. IRC-21-38.

[52] Harden, A. L., Kang, Y-S., *et al*. (2021) Preliminary Sex-specific Relationships between Peak Force and Cortical Bone Morphometrics in Human Tibiae Subjected to Lateral Loading. *Proceedings of the IRCOBI Conference*, online: pp.232–248. IRC-21-33.

[53] Hunter, R. L., Haverfield, Z., Agnew, A. M. (2021) Investigation of Sex-specific Effects on Variation in Cortical Bone Morphometrics of the Radius. *Proceedings of the IRCOBI Conference*, online: pp.288–307. IRC-21-37.

[54] Yoganandan, N., Arun, M. W. J., Pintar, F. A. (2014) Normalizing and scaling of data to derive human response corridors from impact tests. *Journal of Biomechanics*, **47**(8): pp.1749–1756. doi:10.1016/j.jbiomech.2014.03.010.

[55] Saltelli, A., Ratto, M., *et al.* (2007) Global Sensitivity Analysis. The Primer. Chichester, UK: John Wiley & Sons, Ltd. doi:10.1002/9780470725184.

[56] Schneider, L. W., Robbins, D. H., Pflueg, M. A., Snyder, R. G., (1983) Development of Anthropometrically Based Design Specifications for an Advanced Adult Anthropomorphic Dummy Family, Volume 1, Final Report UMTRI-83-53-1. University of Michigan Transportation Research Institute, Ann Arbor, MI.

[57] Burkhart, T. A., Andrews, D. M., Dunning, C. E. (2013) Finite element modeling mesh quality, energy balance and validation methods: A review with recommendations associated with the modeling of bone tissue. *Journal of Biomechanics*, **46**(9): pp.1477–1488. doi:10.1016/j.jbiomech.2013.03.022.

[58] Human Accom and Design Devices Stds Comm (2021), SAE J826_202106: Devices for Use in Defining and Measuring Vehicle Seating Accommodation; SAE International: Warrendale, PA, USA, 2021.

Appendix A
OCCUPANT ANTHROPOMETRY ANALYSIS

Statistical analysis in the NASS GES database was performed to identify the most frequent age of occupants involved in crashes regardless of injury level. The filtering criteria used for the analysis can be seen in A.I.

TABLE A.I
NASS FILTERING CRITERIA

Variable	Value	Interpretation
PER_TYP	2, 3	Passenger of a Motor Vehicle in Transport, Occupant of a Motor Vehicle Not in Transport
BODY_TYP	< 30	Automobiles, automobile derivatives, utility vehicles, van-based light trucks (≤10,000 lbs GVWR)
SEAT_POS	13	Front Seat – Right Side
PERSON.AGE	>= 20 AND <= 120	Occupants aged between 20 and 120 yo
SEX	1, 2	Male, Female

The results of the analysis indicate that the mean age of occupants involved in crashes between the years 2011 and 2015 was 41 years old (yo) (A.1), with the average age of male and female occupants being 38 yo and 43 yo, respectively. Hence, 40 yo was selected as the target age for the morphed HBMs.

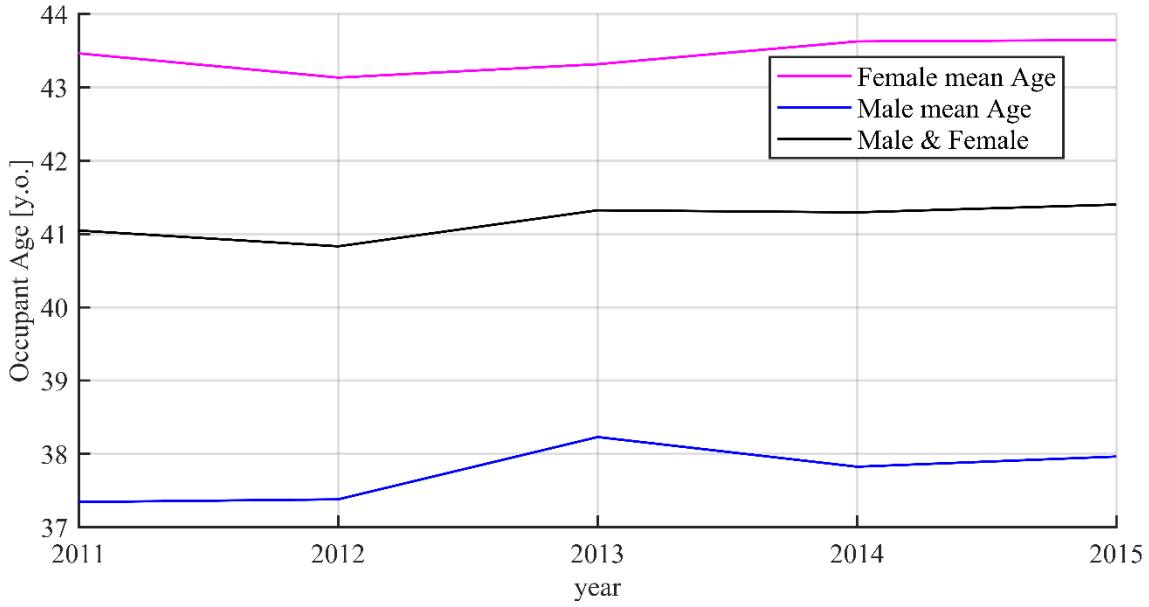

Fig. A.1. The mean age of injured front-seat passengers from the NASS GES database are visualised. Throughout 2011–2015, the mean age is approximately 43 yo and 38 yo for female and male occupants, respectively. The mean age, irrespective of sex, was approximately 41 yo.

To identify the BMI and stature distribution of the population, the National Health and Nutrition Examination Survey (NHANES) database for the years 2013–2016, weighted to represent the US population, was analysed. The univariate medians of the female and male populations were used as the baseline target anthropometries (Table A.II).

To define the borders of the sampling space, lines that join points of the sampling space (Stature, BMI) with the same probability density value (iso-probability lines) covering 90% of the male and female populations were generated (Fig. A.2). The probability density function was estimated using the "Kernel smoothing function estimate for bivariate data" (ksdensity) in MATLAB R2017b (MathWorks, Massachusetts, USA). The surface integral of the probability density function within the iso-probability line describes the percentage of the population contained in the area.

The difference between the median male and median female stature (141 mm) was used to define the grid

spacing for the stature, and 5 kg/m^2 was used as the grid spacing for BMI. An equidistant grid (Fig. A.2) was generated to define the target occupant anthropometries.

TABLE A.II
UNIVARIATE ANALYSIS OF STATURE AND BMI FOR THE WEIGHTED US POPULATION

	Female Population (n=5571)		Male Population (n=5221)	
Stature	1476 mm	p2.8	1617 mm	p3.5
	1617 mm	**p50**	**1758 mm**	**p50**
	1758 mm	p97.9	1899 mm	p97.7
BMI	18 kg/m^2	p1.2	18 kg/m^2	p0.9
	23 kg/m^2	p20.7	23 kg/m^2	p13.8
	28 kg/m^2	**p49**	**28 kg/m^2**	**p50.3**
	33 kg/m^2	p72	33 kg/m^2	p79
	38 kg/m^2	p86.7	38 kg/m^2	p92.5

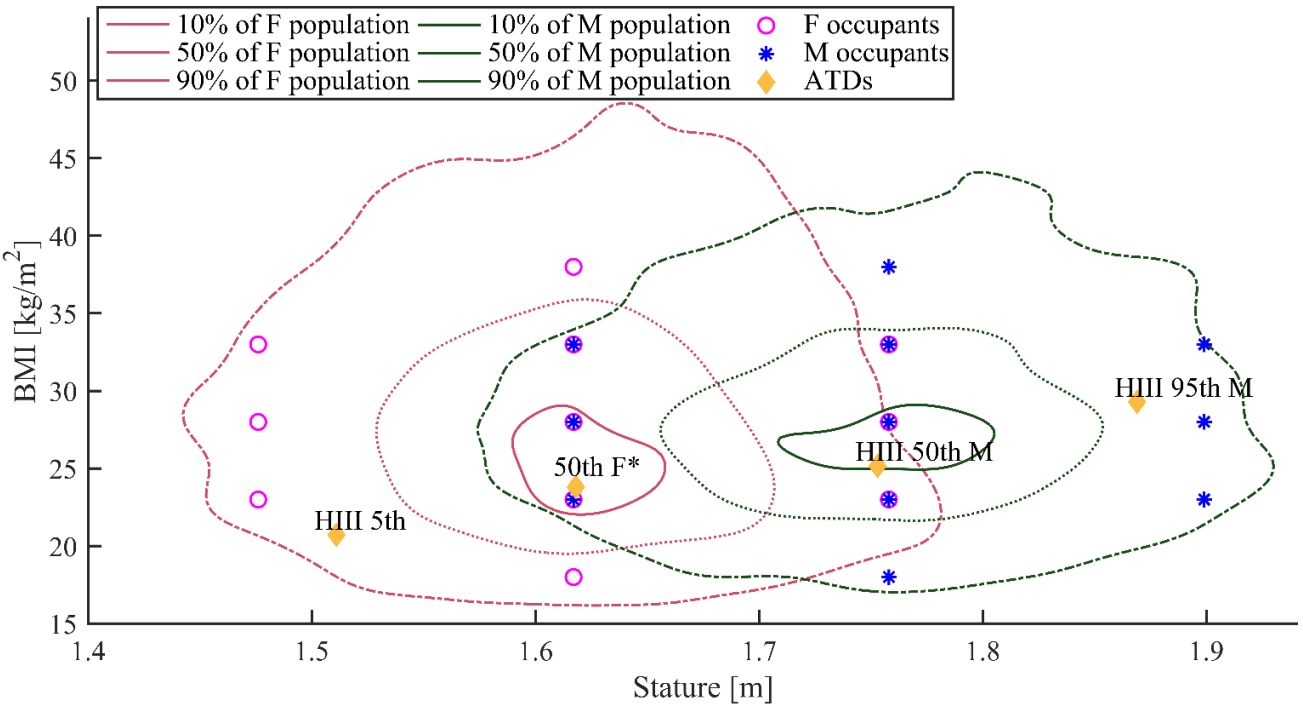

Fig. A.2. The bivariate distribution of the US population is illustrated using iso-probability contours lines for the female (in red) and male (in green) subpopulations. The contour lines define the borders that contain 10% (solid line), 50% (dotted line) and 90% of the subpopulations. The selected occupant sizes (BMI and stature) are visualised with magenta and circles and blue stars for the female and male populations. Additionally, the dimensions of the Hybrid-III Anthropomorphic Test Devices and the 50th percentile female in accordance with Schneider *et al.* [56] are included in yellow diamonds for easy comparison with the selected anthropometries.

The anthropometric properties of the baseline and morphed HBMs can be seen in Table A.IV. Moreover, the element quality of the morphed HBMs was assessed by counting the number of elements that violated selected element quality criteria (EQC) [57], seen in Table A.III. The number of elements violating the EQC was normalised with respect to the number of elements violating the EQC of the baseline HBM, to derive the model quality presented in Table A.IV. Hence, a model quality of 148% means that the number of elements violating the EQC is increased by 48% compared to the baseline HBM. This also means that higher numbers indicate worse mesh quality, and have been colour coded (in red) in Table A.IV to highlight this.

Additionally, at the end of the occupant positioning stage, the contact force was divided by the occupant's weight to assess whether equilibrium was reached; the minimum and maximum "equilibrium calculation" values achieved for all seat adjustments can be seen in Table A.IV.

TABLE A.III
ELEMENT QUALITY CRITERIA LIMITS

Volume & Shells				Volume						Shells			
				Tetra-		Penta-		Hexa-		Quad-		Tria-	
Jacobian	Aspect Ratio	Skewness	Warping	min angle	max angle	min angle	max angle	min angle	max angle	min angle	max angle	min angle	max angle
0.3	10	60	20	20	150	20	160	20	160	20	160	30	120

TABLE A.IV
MEASUREMENTS, ELEMENT QUALITY, AND EQUILIBRIUM WITH SEAT FOR THE MORPHED HBMS

#	Sex	Stature (mm)	Weight (kg)	BMI	Age	Model Quality	Head Properties				Equilibrium	
							Mass (kg)	Inertia (kg * mm²) Ixx	Iyy	Izz	Min.	Max.
SAFER HBM v9.0.1	*M*	1750	77	25	N/A	100%	4.682	23173	20876	16634	N/A	
1	F	1476	50.11	23	40	148%	4.092	18925	16938	13246	155%	205%
2	F	1476	61.00	28	40	149%	4.166	19686	17643	13756	147%	188%
3	F	1476	71.89	33	40	143%	4.272	20589	18486	14321	143%	180%
4	F	1617	47.06	18	40	156%	4.238	20579	18388	14152	149%	160%
5	F	1617	60.14	23	40	150%	4.335	21390	19120	14697	139%	158%
6	F	1617	73.21	28	40	141%	4.432	22242	19904	15258	135%	144%
7	F	1617	86.28	33	40	140%	4.542	23253	20840	15880	134%	157%
8	*F*	1617	99.36	38	40	141%	4.675	24322	21774	16545	144%	165%
9	*F*	1758	71.08	23	40	144%	4.613	24167	21573	16301	141%	172%
10	F	1758	86.54	28	40	137%	4.714	25117	22444	16915	135%	169%
11	F	1758	101.99	33	40	132%	4.827	26249	23485	17600	135%	199%
12	*M*	1617	60.14	23	40	153%	4.471	22779	20354	15781	133%	143%
13	*M*	1617	73.21	28	40	133%	4.577	23676	21156	16436	124%	139%
14	*M*	1617	86.28	33	40	129%	4.698	24720	22108	17156	117%	131%
15	*M*	1758	55.63	18	40	155%	4.646	24798	22104	16800	144%	158%
16	*M*	1758	71.08	23	40	141%	4.747	25617	22861	17445	128%	140%
17	*M*	1758	86.54	28	40	141%	4.895	26750	23780	18283	127%	138%
18	*M*	1758	101.99	33	40	124%	4.98	27779	24805	18946	124%	144%
19	*M*	1758	117.44	38	40	125%	5.106	29025	25939	19774	115%	169%
20	*M*	1899	82.94	23	40	136%	5.039	28797	25669	19276	122%	141%
21	*M*	1899	100.97	28	40	124%	5.152	29902	26656	20049	124%	156%
22	*M*	1899	119.00	33	40	127%	5.3	31209	27825	20917	126%	184%

TABLE A.V
PARAMETERS INVESTIGATED AND BASELINE VALUES

Parameter	Range	Baseline value
Backrest	25°, 30°	25°
Fore-aft (%)	0% (only for statures ≤1617), 20% (only for statures ≤1758), 40%, 60%, 80%, 100% for all statures	40%
BMI (kg/m²)	23, 28, 33 for all stature levels 18 and 38 for females and males with "baseline" stature	28
Stature (mm)	1476, 1617 and 1758 for females, 1617, 1758, 1899 for males	1617 for Females, 1758 for Males
Sex	Female, Male	Male

Appendix B
HBM Positioning Method

An automated occupant positioning method, comprising two steps, was used to position the HBM. First, the HBM target position was determined using a set of rules, with respect to the geometrical constraints of the vehicle. Then, a positioning (pre)simulation was performed to establish the positioned HBM and squashed seat.

The HBM target position was calculated by performing a set of sequential rigid body translations and rotations to optimise a set of predefined criteria (Table B.I), using an in-house tool, developed in MATLAB R2017b (MathWorks, Massachusetts, USA). Target positions for certain anatomical landmarks were extracted from the calculated HBM target position and were used to set up the positioning (pre)simulations. Examples of the HBM target position calculation are illustrated in Fig. B.1, for occupants of different sizes in different seat adjustments.

Table B.I
Occupant positioning Step 1: Rules and Actions to Define the HBM Target Position

Body Region	Action	
H-Point	I.	Move the HBM H-point to the H-Point Manikin location (SAE J866, [58]).
Torso	II.	Rotate the occupant around the H-Point until it the torso in contact with the backrest.
Lower extremities	III.	Rotate the thigh, calf, and feet around the Y-axis until:
		the thighs are in contact with the seat base,
		and the feet are as low and forward as possible while in contact with the carpet.
Upper extremities	IV.	Rotate the shoulders around Y until the arms contacts the backrest.
	V.	Rotate the elbows around Y until the hands contacts the thighs.

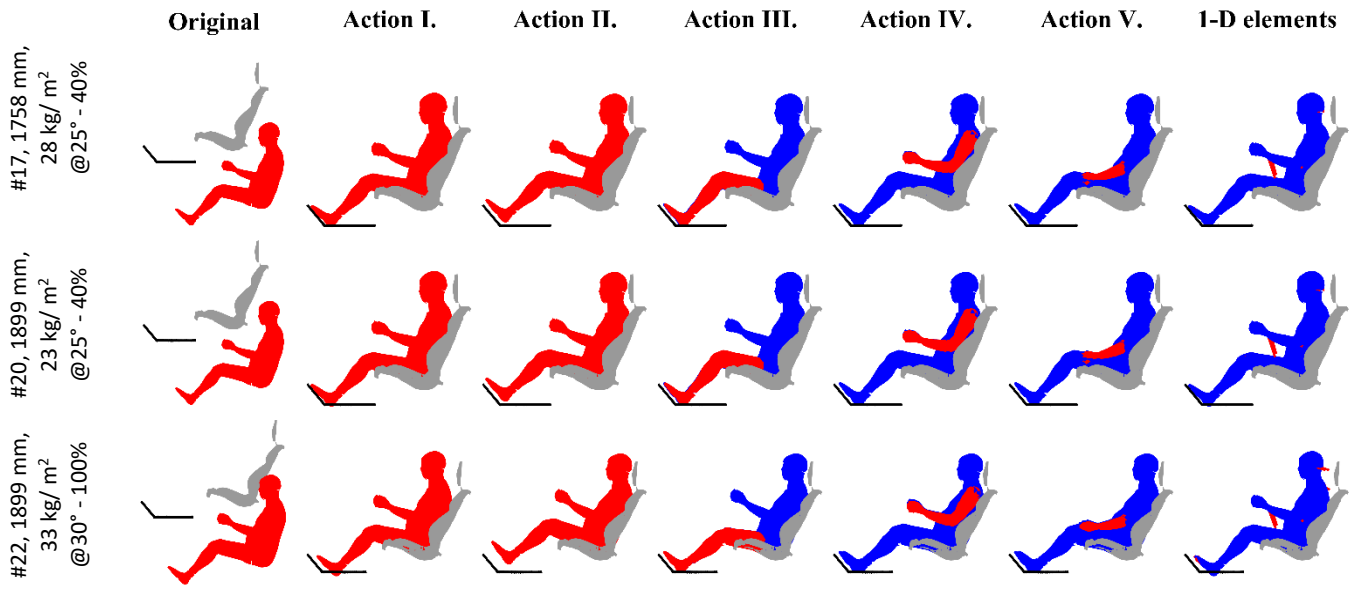

Fig. B.1. Calculation of the HBM target position; examples with HBMs of different sizes positioned in different seat adjustments. On the left, the HBM and the relevant vehicle geometrical constraints (carper and seat) can be seen. A set of rigid body rotations and translations – Actions I–V, (Table B.I) – are performed to define the desired occupant position. On the right, the resulting 1-D elements are illustrated in red.

In the positioning (pre)simulations, the marionette method [40] was used to move the HBM to the calculated target position, using one-dimensional elements to pull the anatomical landmarks into their calculated target positions. The positioning (pre)simulation had a duration of 700 ms and consisted of two stages.

First (Fig. B.2), a force 70–350 N was applied using the one-dimensional elements for 450 ms. Simultaneously with the pulling of the occupant landmarks into position, the vehicle geometrical constraints were also moved into position. The relevant vehicle surfaces that come into contact with the HBM (in this case, the seat, the floor and the IP) started 150 mm away (in the X- and Z- directions) from the HBM and were moved into their original position. In the second stage, after 450 ms (Fig. B.3), the force of the elements was set to 0 N, and the HBM was

allowed to reach equilibrium with the vehicle interior. Gravity was applied throughout the entire simulation to generate the appropriate contact forces and deform the seat cushion.

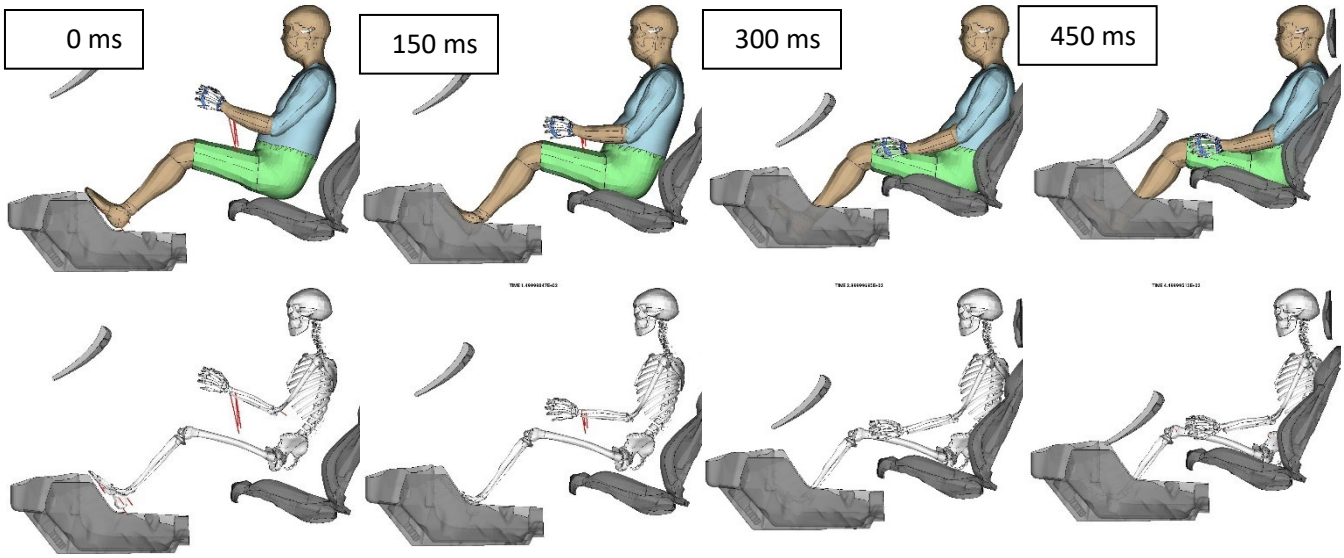

Fig. B.2. HBM positioning, stage 1: the selected HBM landmarks are pulled into the target position by the 1-D elements (red), while simultaneously the vehicle geometrical constraints (seat and carpet) are moved into position.

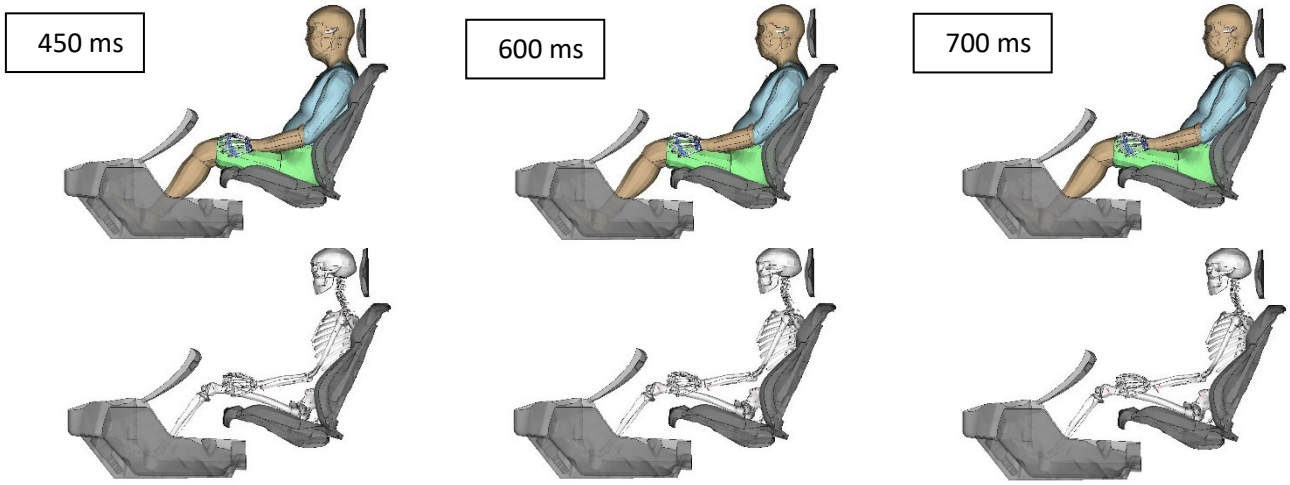

Fig. B.3. HBM positioning, stage 2: the 1-D elements (red) stop applying force, and the HBM is allowed to reach equilibrium with the vehicle environment.

The contact force between the IP and the HBM's knees was monitored to determine whether an occupant sitting in the seat adjustment is realistic, with 0.5 kN being the threshold. HBMs with stature above 1617 mm and 1758 mm could not be positioned in the 0% and 20% fore-aft seats, respectively. The stresses produced during the positioning stage (Fig. B.4) were not retained for the HBM but were reinitialised for the foam of the seat (using the INITIAL_FOAM_REFERENCE option of LS-DYNA).

Fig.B.4. HBM positioning, seat squashing. The contact between the occupant and the seat deforms the seat foam. In the 300–450 ms time interval, the occupant is pulled into position. Between 450 ms and 700 ms, the external force is stopped and the HBM is allowed to reach equilibrium with the seat under gravity loading.

Initial Distance to Vehicle Interior, Posture, and Belt Fit

The HBM H-Point position relative to the seat was influenced by BMI, sex and stature. Occupants with BMI 38 kg/m^2 were positioned 16 mm higher and 12 mm more forward, while occupants with BMI 18 kg/m^2 were 10 mm lower and 3 mm more backward compared to occupants with nominal BMI. Female occupants were 20 mm higher and 7 mm more forward, and the H-point of shorter (1476 mm) occupants was 9 mm more forward.

Additionally, the fore-aft position and backrest angle altered the distance between the occupant and the interior constraints, such as the glovebox and the dashboard (through which the frontal airbag is deployed). The knee-to-dashboard (and -glovebox) distance was affected by the fore-aft position (+125 mm when full rearward, -75 mm when full forward). The knees of underweight occupants were 21 mm further away from the dashboard, while obese occupants (38 kg/m^2) were 29 mm closer, and the knees of female occupants were 16 mm closer to the dashboard compared to males of the same stature and BMI. Being 141 mm taller was associated with a 60 mm reduction in the distance between knees and dashboard. However, short (1476 mm) females were the exception of that, with their knees being 38 mm closer to the dashboard compared to females of average stature (1617 mm). As compared to the nominal fore-aft position, the head-to-dashboard distance was 150 mm longer when the seat was in the most rearward position and 100 mm shorter when in the most forward position. Reclining the backrest increased the head distance by 53 mm.

In Table F.I to Table F.III, the median change of analysed response is reported, along with the IQR in parenthesis.

TABLE B.II
INITIAL DISTANCE TO VEHICLE INTERIOR

Backrest		30° vs. 25°		
Head	Head to dashboard [mm]	*53 (51,55)		
Fore-aft		Full rearward vs. Nom.	Full forward vs. Nom.	
Lower Extremities	Right Knee to glovebox trim distance [mm]	*124 (121,126)	*-75 (-79,-71)	
	Left Knee to glovebox trim distance [mm]	*121 (118,123)	*-71 (-75,-70)	
Head	Head to dashboard [mm]	*152 (150,153)	*-101 (-102,-100)	
BMI		18 vs. 28	38 vs. 28	
Pelvis	Pelvis CoG to Seat H-Point (Mannequin measurement) X-dist. [mm]	*3 (1,7)	*-12 (-14,-9)	
	Pelvis CoG to Seat H-Point (Mannequin measurement) Z-dist. [mm]	*-10 (-11,-4)	*16 (14,17)	
Lower Extremities	Right Knee to glovebox trim distance [mm]	*21 (18,24)	*-30 (-31,-27)	
	Left Knee to glovebox trim distance [mm]	*20 (18,24)	*-29 (-31,-26)	
Stature		1617 vs. 1476	1758 vs. 1617	1899 vs. 1758
Pelvis	Pelvis CoG to Seat H-Point (Mannequin measurement) X-dist. [mm]	*9 (6,12)	*-4 (-8,-1)	0 (-4,5)
	Pelvis CoG to Seat H-Point (Mannequin measurement) Z-dist. [mm]	0 (-3,2)	*3 (1,7)	*3 (2,4)
Lower Extremities	Right Knee to glovebox trim distance [mm]	*-39 (-45,-32)	*-59 (-63,-57)	*-61 (-63,-59)
	Left Knee to glovebox trim distance [mm]	*-39 (-48,-36)	*-59 (-62,-56)	*-61 (-63,-59)
Sex		Female vs. Male		
Pelvis	Pelvis CoG to Seat H-Point (Mannequin measurement) X-dist. [mm]	*-7 (-10,-3)		
	Pelvis CoG to Seat H-Point (Mannequin measurement) Z-dist. [mm]	*20 (16,21)		
Lower Extremities	Right Knee to glovebox trim distance [mm]	*-19 (-24,-17)		
	Left Knee to glovebox trim distance [mm]	*-19 (-23,-17)		

The pelvic angle was 3.8° more reclined when the backrest was adjusted to 30°. Females had a median increase in the pelvic angle of 7.5° when compared to males of the same stature and BMI. That change was even larger (8.6°) for females with a stature of 1756 mm. A 1.7° more reclined angle was seen for obese occupants. However, no considerable change in the pelvic angle of underweight occupants was observed. Similarly, stature was in general not associated with altered pelvic angle, except for short (1476 mm) females, which presented a 2° more reclined pelvis.

Reclining the backrest resulted in a median change of the torso pitch angle of the HBMs of 5.5°. BMI influenced the torso pitch angle with obese occupants (38 kg/m^2) showing 0.9° less reclined torso and underweight occupants showing 1.3° more reclined torso. Small females, with a stature of 1476 mm, were associated with an increase of the torso pitch angle by 3.3° as the pelvis was more forward, while taller males (1899 mm) showed reduced torso pitch angle by 1.7°. The femurs were, on average, 1.7° less elevated for female occupants compared to males, as the pelvis was located higher.

TABLE B.III
INITIAL POSTURE

Backrest		30° vs. 25°		
	Init. Pelvis Y-rotation [°]	*3.8 (3.3,4.1)		
	Init. Torso Y-rotation [°]	*5.5 (5.2,5.8)		
BMI		18 vs. 28		38 vs. 28
	Init. Pelvis Y-rotation [°]	0.2 (-0.2,0.8)		*1.7 (1.6,2)
	Init. Torso Y-rotation [°]	*1.3 (0.7,1.7)		*-0.9 (-1.7,0.3)
	Right Femur Elevation [°]	*-1.2 (-1.1,-1.4)		*1.7 (2,1.5)
	Left Femur Elevation [°]	*-1.3 (-1.4,-1.1)		*1.5 (1.2,1.9)
Stature		1617 vs. 1476	1758 vs. 1617	1899 vs. 1758
	Init. Pelvis Y-rotation [°]	*-2 (-3,-0.7)	-0.3 (-1.3,0.9)	*0.3 (0,0.6)
	Init. Torso Y-rotation [°]	*-3.3 (-3.9,-2.8)	*-0.8 (-1.4,-0.1)	*-1.8 (-2.3,-0.9)
Sex		Female vs. Male		
	Init. Pelvis Y-rotation [°]	*7.5 (6.2,8.5)		
	Right Femur Elevation [°]	*-1.7 (-1.8,-1.5)		
	Left Femur Elevation [°]	*-1.7 (-1.8,-1.4)		

The initial belt fit was affected by all of the investigated parameters. The midpoint of the lap-belt was positioned 40 mm more backwards and 15 mm lower relative to the ASIS for underweight occupants, while it was 60 mm more forward and 40 mm higher for obese occupants (38 kg/m^2) compared to occupants of nominal BMI (Fig. F.1). The lap-belt was 12 mm lower, relative to the ASIS, for female compared to male occupants of the same stature and BMI.

For the shoulder-belt path, measured at the sternum at the 6th rib height and the acromial end of the clavicle, BMI was especially influential over the shoulder-belt path (Fig. F.2). The belt was 47 mm more forward and 31 mm more inboard for obese occupants, while it was 16 mm closer to the sternum longitudinally and 6 mm more outboard. Additionally, the fore-aft position of the seat altered the longitudinal distance between the clavicle and the shoulder-belt by up to 38 mm. Similarly, reclining the backrest increased the longitudinal distance of the belt by 16 mm and pushed it 4 mm inboard. For female occupants, a general trend was observed with the belt being 19 mm more outboard (closer to the acromion) and 16 mm more forward at the sternum compared to males (Fig. F.3). Finally, increasing the stature by 141 mm resulted in up to 20 mm more outboard positioned belt.

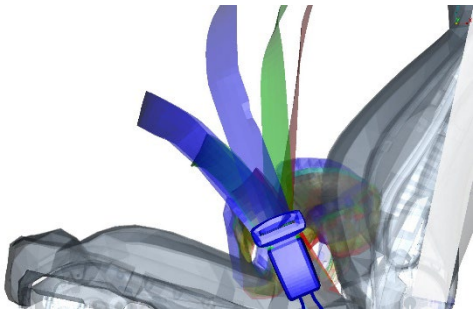

Fig. B.5. The initial lap-belt fit relative to the pelvis is seen. Three male occupants, with stature of 1758 mm and BMI of 18 kg/m^2 (red), 28 kg/m^2 (green) and 38 kg/m^2 (blue) are visible. The lap-belt is more forward and higher relative to the Anterior Superior Iliac Spine (ASIS) for increased BMI, and vice versa for reduced BMI.

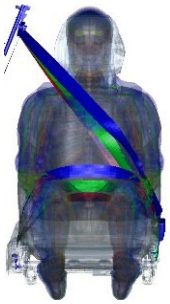

Fig. B.6. The initial shoulder-belt fit for three male occupants, with a stature of 1758 mm and BMI of 18 kg/m^2 (red), 28 kg/m^2 (green) and 38 kg/m^2 (blue), is visible. The shoulder-belt is more medial relative to the clavicle for increased BMI, and vice versa for reduced BMI.

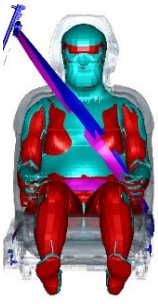

Fig. B.7. The initial shoulder-belt fit is compared between a female (red/magenta) and male (cyan/blue) occupant, with a stature of 1617 mm and BMI of 28 kg/m^2. The belt is 19 mm more lateral relative to the clavicle for the female occupant.

TABLE B.IV
INITIAL BELT FIT

Backrest		30° vs. 25°		
Lap Belt	Left (Buckle) ASIS to Midpoint of Lap Belt, Longitudinal [mm]	*-3 (-7,-1)		
	Left (Buckle) ASIS to Midpoint of Lap Belt, Vertical [mm]	*4 (2,7)		
	Right (Anchor) ASIS to Midpoint of Lap Belt, Longitudinal [mm]	*-4 (-6,-1)		
	Right (Anchor) ASIS to Midpoint of Lap Belt, Vertical [mm]	*4 (1,6)		
Shoulder Belt	Distal Clavicle to Shoulder Belt, Longitudinal Distance [mm]	*16 (8,21)		
	Distal Clavicle to Shoulder Belt, Lateral Distance [mm]	*4 (1,9)		
	Belt Webbing Length [mm]	*20 (14,25)		
Fore-aft		Full rearward vs. Nom.	Full forward vs. Nom.	
Shoulder Belt	Distal Clavicle to Shoulder Belt, Longitudinal Distance [mm]	*38 (32,46)	*-12 (-16,-6)	
	Distal Clavicle to Shoulder Belt, Lateral Distance [mm]	*-2 (-6,1)	-2 (-7,1)	
	Belt Webbing Length [mm]	*-62 (-71,-57)	*60 (56, 66)	
BMI		18 vs. 28	38 vs. 28	
Lap Belt	Left (Buckle) ASIS to Midpoint of Lap Belt, Longitudinal [mm]	*-40 (-44,-38)	*61 (59,63)	
	Left (Buckle) ASIS to Midpoint of Lap Belt, Vertical [mm]	*-16 (-32,-10)	*44 (42,46)	
	Right (Anchor) ASIS to Midpoint of Lap Belt, Longitudinal [mm]	*-45 (-47,-44)	*62 (59,63)	
	Right (Anchor) ASIS to Midpoint of Lap Belt, Vertical [mm]	*-14 (-32,-7)	*40 (38,42)	
Shoulder Belt	Sternum (Mid @6th rib) to Shoulder Belt, Longitudinal Distance [mm]	*-17 (-19,-10)	*48 (31,60)	
	Sternum (Mid @6th rib) to Shoulder Belt, Lateral Distance [mm]	6 (-16,24)	*31 (22,45)	
	Distal Clavicle to Shoulder Belt, Longitudinal Distance [mm]	*-22 (-24,-20)	-1 (-15,12)	
	Distal Clavicle to Shoulder Belt, Lateral Distance [mm]	*36 (27,48)	*18 (9,29)	
	Belt Webbing Length [mm]	*-117 (-124,-114)	*264 (278,250)	
Stature		1617 vs. 1476	1758 vs. 1617	1899 vs. 1758
Lap Belt	Left (Buckle) ASIS to Midpoint of Lap Belt, Longitudinal [mm]	*12 (8,15)	*4 (0,7)	*6 (4,11)
	Left (Buckle) ASIS to Midpoint of Lap Belt, Vertical [mm]	*-5 (-7,-2)	*3 (0,4)	*3 (2,4)
	Right (Anchor) ASIS to Midpoint of Lap Belt, Longitudinal [mm]	*10(8,15)	*5 (2,7)	*8 (6,10)
	Right (Anchor) ASIS to Midpoint of Lap Belt, Vertical [mm]	*-4 (-6,-2)	*3 (1,4)	*3 (2,5)
Shoulder Belt	Sternum (Mid @6th rib) to Shoulder Belt, Longitudinal Distance [mm]	0 (-1,2)	*4 (2,6)	*4 (3,6)
	Sternum (Mid @6th rib) to Shoulder Belt, Lateral Distance [mm]	*-11 (-15,-6)	*-10 (-15,-4)	*-10 (-14,-8)
	Belt Webbing Length [mm]	*16 (8,46)	*37(28,56)	*31 (26,42)
Sex			Female vs. Male	
Lap Belt	Left (Buckle) ASIS to Midpoint of Lap Belt, Longitudinal [mm]		*2 (0,5)	
	Left (Buckle) ASIS to Midpoint of Lap Belt, Vertical [mm]		*-10 (-11,-8)	
	Right (Anchor) ASIS to Midpoint of Lap Belt, Longitudinal [mm]		*4 (2,5)	
	Right (Anchor) ASIS to Midpoint of Lap Belt, Vertical [mm]		*-11 (-13,-11)	
Shoulder Belt	Sternum (Mid @6th rib) to Shoulder Belt, Longitudinal Distance [mm]		*16 (11,38)	
	Sternum (Mid @6th rib) to Shoulder Belt, Lateral Distance [mm]		*-28 (-34,-19)	
	Distal Clavicle to Shoulder Belt, Longitudinal Distance [mm]		-5 (-10,6)	
	Distal Clavicle to Shoulder Belt, Lateral Distance [mm]		*-19 (-25,-15)	
	Belt Webbing Length [mm]		*24 (13,53)	

Appendix C
ANALYSED RESPONSES

Table C.I contains the anatomical landmarks and cross-sections that were included for every body region analysed. Additionally, the depiction of the anatomical landmarks and cross-sections of the baseline HBM is available in the supplementary material of [22].

TABLE C.I
ANATOMICAL LANDMARKS EXCURSION (EXC.) (BLACK), ANGLES (BLUE), VELOCITIES (RED), AND CROSS-SECTION LOADS (GREEN)

Pelvis	Spine	Torso	Head	Lower extremities - Bilateral	Upper extremities - Bilateral
Pubic symphysis exc.	L1-L5 vertebra exc.	Sternum (mid at 1st rib height) exc.	Centre of Gravity (CoG) exc.	Femoral head exc.	Acromion exc.
Bilateral iliac crest exc.	T1-12 vertebra exc.	Sternum (mid at 6th rib height) exc.	Most Superior Point exc.	Patella exc.	Olecranon exc.
Bilateral ASIS exc.	C1-C7 vertebra exc.	Sternum X- , Y- , Z- , res. velocity	Nasion exc.	Distal tibia exc.	Distal radius exc.
Sacrum (Superior, Anterior & Posterior) exc.	Upper Neck load	Torso X- , Y- , Z- angle	Inion exc.	Calcaneus exc.	Thumb distal phalanx exc.
Pelvic X- , Y- , Z- angle	Lower Neck load		Bilateral Porion exc.	First distal phalanx exc.	Distal humerus load
Bilateral pubic rami load	L1-L5 Vertebra load		Bilateral Orbitale exc.	Distal femur load	Proximal humerus load
Bilateral Sacroiliac (SI) joint load			Head X- , Y- , Z- angle	Proximal tibia load	Distal forearm load
Bilateral ASIS load			CoG X- , Y- , Z-, res. velocity	Distal tibia load	

Appendix D
GLOBAL SENSITIVITY METHOD

- Let $f({}^1x, \dots, {}^ix, \dots, {}^kx)$ be the evaluated function with k input variables.
- Assuming that the input range of the $i-th$ input variable is $\left({}^i_{min}x, {}^i_{max}x\right)$,discrete steps ${}^i\delta$ are chosen for every input variable, dividing the input space of the $i-th$ input variable to a linearly spaced interval. ${}^ix \in \left({}^i_{min}x, {}^i_{min}x + {}^i\delta, \dots, {}^i_{max}x\right)$.
- The combination of the linearly spaced intervals for all variables generates an equidistant grid in the k-dimensional hypercube.
- This approach allows for OAT (one-at-a-time) comparisons for every input variable at every point of the grid.
- The change of the response due to changing the input variable i to a (from the baseline level ${}^i_bx$) is calculated by:

$$ {}^i_a\Delta\mathrm{f} = {}^i_a\Delta\mathrm{f}_{\left({}^1x,\dots,{}^i_ax,\dots,{}^kx\right)\to({}^1x,\dots,{}^i_bx,\dots,{}^kx)} = f\left({}^1x, \dots, {}^i_ax, \dots, {}^kx\right) - f({}^1x, \dots, {}^i_bx, \dots, {}^kx) $$

- The local sensitivity of the $i-th$ variable in the $\left({}^1x, \dots, {}^i_ax, \dots, {}^kx\right)$ point of the hyperspace is given by:

$$ LS^i_a = LS^i_{\left({}^1x,\dots,{}^ix,\dots,{}^kx\right)\to({}^1x,\dots,{}^i_bx,\dots,{}^kx)} = \frac{{}^i_a\Delta\mathrm{f}}{{}^i_ax - {}^i_bx} $$

- The calculation is repeated at every point of the hyperspace where ${}^ix \neq {}^i_bx$.
  This generates a data sample of local sensitivities for all points of the grid.

$$ LS^{\{i\}} = \left[LS^i_a\right]\forall({}^1x, {}^2x, \dots, {}^kx) $$

- Calculating the median and Interquartile Range (IQR) generates the m^i, m^{*i} and IQR^i
  - $\mathrm{m}^i = P_{50}(LS^{\{i\}})$
  - $\mathrm{IQR}^i = P_{75}\left(LS^{\{i\}}\right) - P_{25}(LS^{\{i\}})$
- Let $LS^{\{i\}}_{j=l}$ be the subset of $LS^{\{i\}}$, where the input variable j has a value l. Following the above equations, $m^i_{j=l}$, $m^{*i}_{j=l}$, and $IQR^i_{j=l}$ can be calculated.
- The Wilcoxon signed rank test can be calculated on the $LS^{\{i\}}$. That tests the hypothesis that the local sensitivities come from a distribution with median different than 0, indicating a consistent trend.
- Deviations between $m^i_{j=l}$, $IQR^i_{j=l}$ and m^i, and IQR^i indicate the presence of interaction effects between the i and j input variable (at the level l, of variable j).

As an example, the effect of changing the fore-aft position of the seat on the peak head resultant speed was investigated. In Table D.I, the sensitivity at the most forward seat position was calculated. For all occupant sizes (that could fit in that specific seat adjustment), the peak head relative speed was calculated (column: Response @x) as well as the response of the reference position (column: Response @reference). The difference between the response at the evaluated position and the reference position is calculated (column: Delta Response). The median change of the change in response of this specific example was -2.44 with IQR of 0.57, and was statistically significant with a p-value, for the two-sided Wilcoxon signed rank test, of 4e-5.

Interaction effects could also be evaluated by generating subgroups, where the 2nd order effect has the same value. In this example, interactions between the fore-aft position and backrest angle were investigated. The groups with backrest angles of 25° and 30° can be seen in green and orange, respectively.

The process was repeated for all values of the evaluated parameter (0%, 20%, 60%, 80% and 100% fore-aft position, in this example) to understand the sensitivity of the evaluated response in the tested range.

TABLE D.I

EXAMPLE OF GSA CALCULATIONS; INFLUENCE OF MOST FORWARD FORE-AFT POSITION TO PEAK HEAD RELATIVE RESULTANT SPEED DURING THE ONCOMING FRONTAL

BMI	Sex	Stature	Backrest	Fore-aft @x	Fore-aft @reference	Response @x	Response @reference	Delta Response
23	Female	1476	25°	0%	40%	7.88	10.88	-3.00
23	Female	1476	30°	0%	40%	9.70	11.99	-2.30
28	Male	1617	25°	0%	40%	8.44	11.22	-2.78
28	Male	1617	30°	0%	40%	10.27	12.54	-2.27
33	Female	1476	25°	0%	40%	7.63	10.49	-2.87
33	Female	1476	30°	0%	40%	9.35	11.73	-2.38
18	Female	1617	30°	0%	40%	10.16	12.24	-2.08
18	Female	1617	25°	0%	40%	8.40	11.20	-2.80
23	Male	1617	30°	0%	40%	10.38	12.59	-2.20
23	Male	1617	25°	0%	40%	8.61	11.36	-2.75
33	Male	1617	30°	0%	40%	10.13	12.58	-2.46
33	Male	1617	25°	0%	40%	8.31	10.99	-2.67
28	Female	1617	25°	0%	40%	8.15	11.06	-2.91
28	Female	1617	30°	0%	40%	10.13	12.31	-2.18
38	Female	1617	25°	0%	40%	8.35	10.77	-2.42
38	Female	1617	30°	0%	40%	9.93	12.13	-2.19
28	Female	1476	25°	0%	40%	7.66	10.75	-3.09
28	Female	1476	30°	0%	40%	9.60	11.83	-2.24
33	Female	1617	30°	0%	40%	10.04	12.26	-2.23
33	Female	1617	25°	0%	40%	8.18	10.95	-2.77
23	Female	1617	25°	0%	40%	8.29	11.17	-2.89
23	Female	1617	30°	0%	40%	10.26	12.35	-2.09
							Median	**-2.44**
							IQR	**0.57**
							p-value	**4.01E-05**

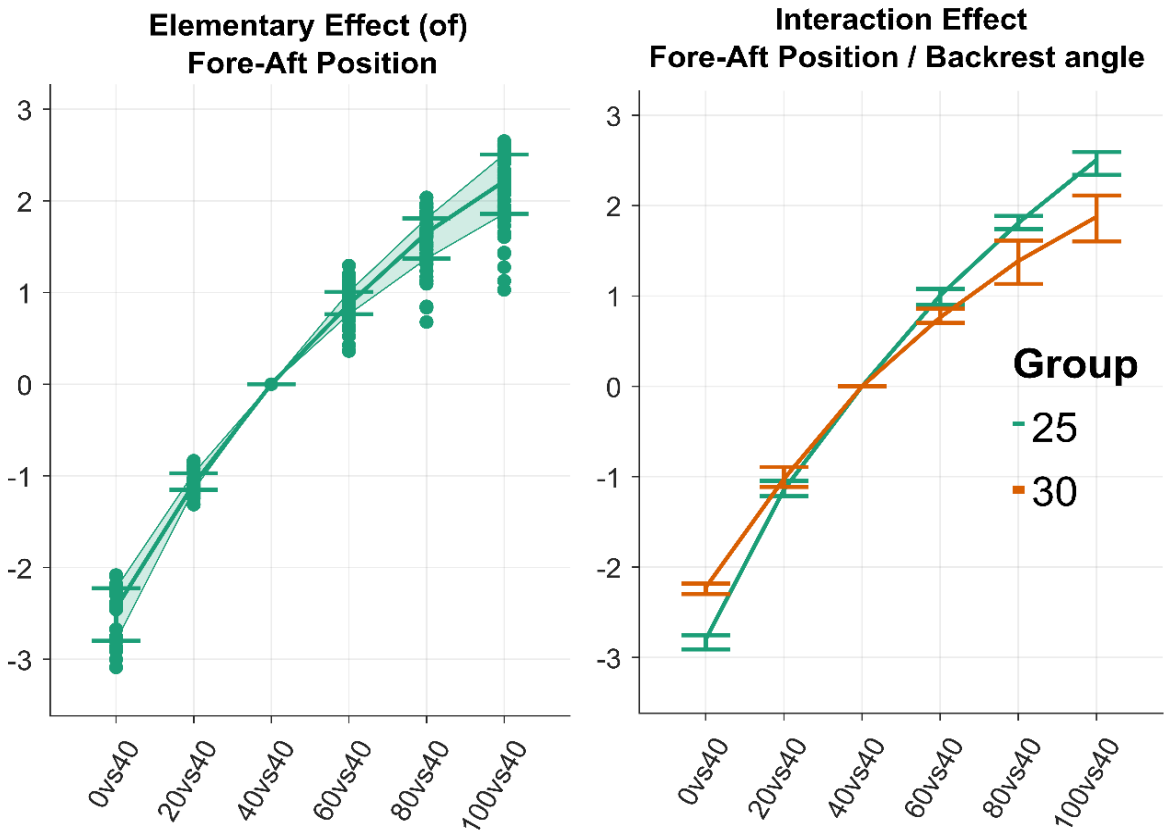

Fig. D.1. Head relative peak resultant velocity during the Oncoming Frontal, depending on the seat's fore-aft position. Positioning the seat in the most forward position results in a 2.44 m/s median reduction of head speed compared to occupants positioned in the nominal fore-aft position. On the right, it can be seen that the seat's backrest angle interacts with the fore-aft adjustment regarding the head's peak velocity. When the seat is in the nominal backrest angle (25 degrees), the fore-aft position is more influential on the head's speed.

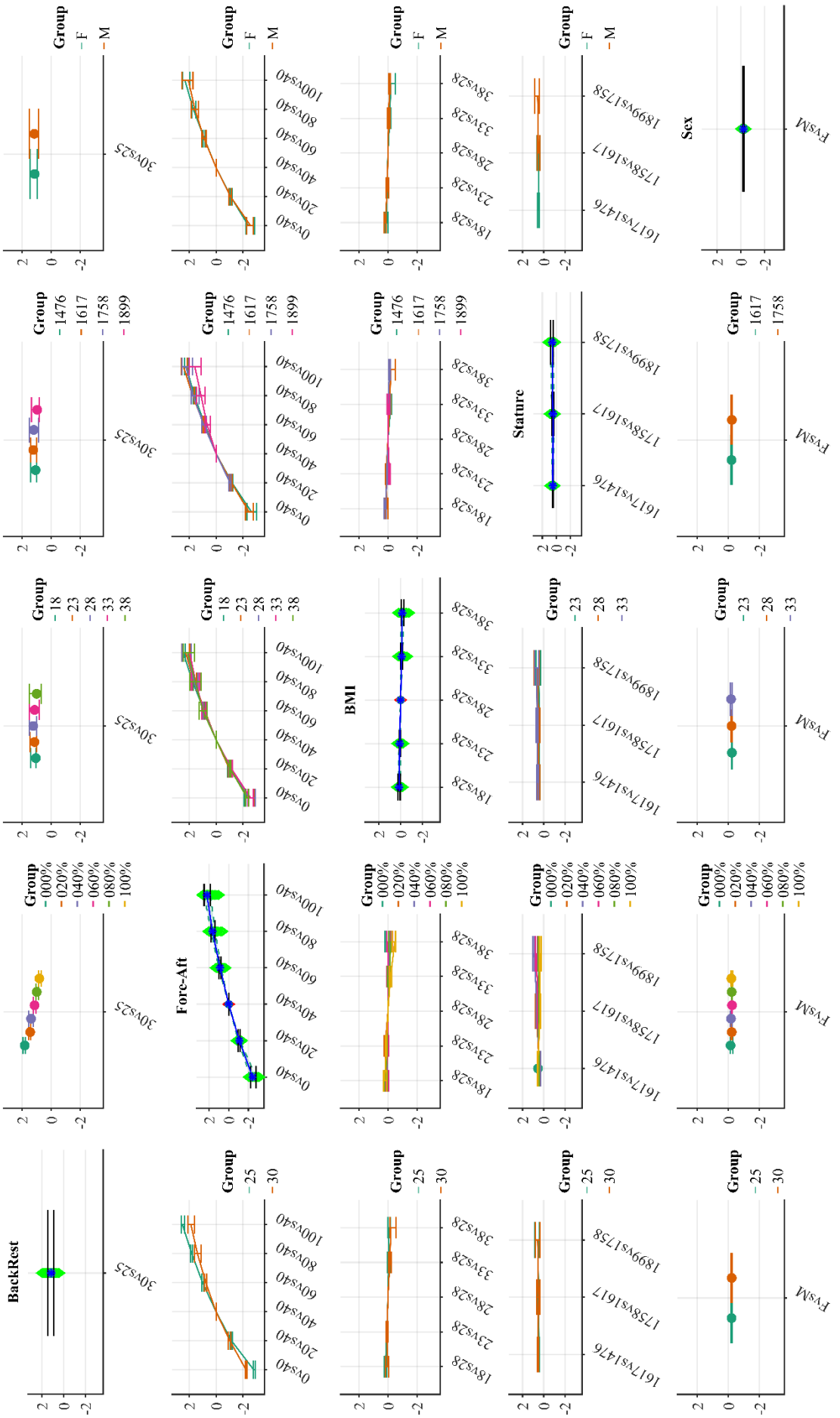

Fig. D.2. Global sensitivity analysis of the head relative peak resultant velocity during the Oncoming Frontal, considering all evaluated parameters. On the diagonal, the elementary effects of the backrest angle, fore-aft position, BMI, stature and sex can be seen. On the off-diagonal effects, the (1st order) interaction effects are plotted.

Appendix E
CORA Calculation Example

As an example, the CORA calculation for the influence of BMI in Pelvis Kinetics during Oncoming Frontal can be seen in Fig. E.1. The median $CORA_{reduction}$ of BMI was [-0.51, -0.30, -0.27, -0.41] for BMI levels [18 kg/m^2, 23 kg/m^2, 33 kg/m^2, 38 kg/m^2], respectively. Therefore, occupants with BMI 18 kg/m^2 were associated with the largest influence over the pelvis kinetics, and the CORA score (CORA = 1- $CORA_{reduction}$) for BMI was 0.49. In a similar fashion, the CORA scores were calculated for all body regions and investigated parameters.

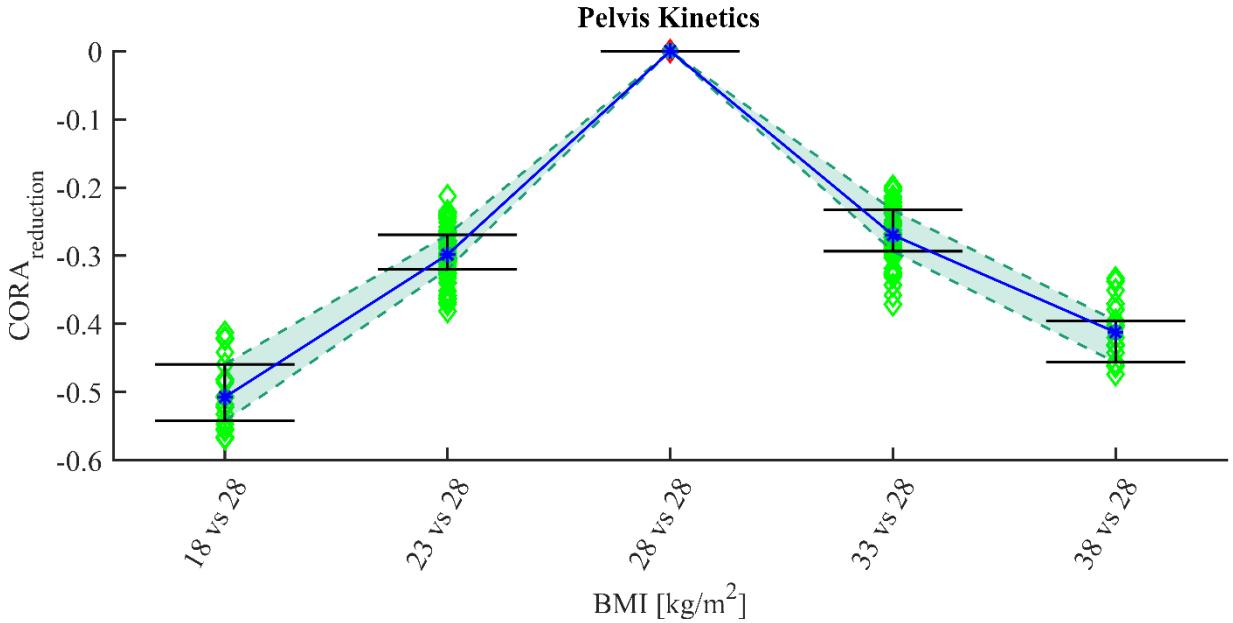

Fig. E.1. The influence of BMI over the pelvis kinetics during the Oncoming Frontal is visualised. It can be seen that the extremes of the evaluated interval for the BMI parameters resulted in the largest median $CORA_{reduction}$ (-0.51 for BMI 18 kg/m^2 and -0.41 for BMI 38 kg/m^2). The reported value is the one with the largest effect (-0.51) and is translated to a CORA score of 0.49.

Appendix F

SIDE IMPACTS – RANKING OF PARAMETERS' INFLUENCE PER BODY REGION'S RESPONSE & KINEMATIC/KINETIC PATTERNS

Near-Side; Ranking of Parameters' Influence – Cross-correlation

In the Near-Side impact (Table F.I), the cross-correlation results indicate that the torso kinematics were affected by the fore-aft position and BMI, with CORA scores of 0.79 and 0.81, respectively. The head kinematics were affected mainly by the fore-aft position of the seat and the stature (0.73) of the occupant. The kinematics of the lower extremities were influenced by the fore-aft position of the seat (0.77), and the occupant's BMI (0.69) and stature (0.71). The upper extremities' kinematics and kinetics were sensitive to variations of all evaluated parameters, with CORA scores between 0.30 and 0.74. The pelvis kinetics had relatively low CORA scores (0.58–0.72) for all parameters, except the backrest angle. The lumbar spine loading was altered by the fore-aft position (0.77) and BMI (0.78), and the cervical spine kinetics were sensitive to the backrest angle (0.64), fore-aft position (0.47), BMI (0.51), stature (0.44) and sex (0.79). Stature was largely influential (0.38) for the lower extremities' kinetics, which was also affected by the fore-aft position (0.52), BMI (0.53) and sex (0.59).

TABLE F.I

NEAR-SIDE CORA RESULTS – ALTERED RESPONSES ARE VISUALISED IN RED

	Kinematics								Kinetics				
	Pelvis	Spine (Lumbar)	Spine (Thoracic)	Spine (Cervical)	Torso	Head	Extremities Lower	Extremities Upper	Pelvis	Spine (Lumbar)	Spine (Cervical)	Extremities Lower	Extremities Upper
Backrest	0.92	0.97	0.96	0.95	0.89	0.80	0.88	0.69	0.83	0.84	0.64	0.69	0.53
Fore-Aft	0.84	0.87	0.85	0.85	0.79	0.73	0.77	0.64	0.72	0.77	0.47	0.52	0.30
BMI	0.82	0.83	0.82	0.84	0.81	0.80	0.69	0.65	0.58	0.78	0.51	0.53	0.35
Stature	0.88	0.93	0.92	0.92	0.84	0.73	0.71	0.72	0.67	0.86	0.44	0.38	0.49
Sex	0.88	0.97	0.97	0.97	0.86	0.87	0.82	0.74	0.68	0.88	0.79	0.59	0.57

Far-Side; Ranking of Parameters' Influence – Cross-correlation

In the Far-Side impact (Table F.II), BMI influenced the pelvis (0.62), spine (lumbar – 0.53, thoracic – 0.61, cervical – 0.7) and head (0.73) kinematics. The lower extremities kinematics were affected by fore-aft position, BMI, stature and sex (0.65–0.8) and the upper extremity kinematics were influenced by all parameters with CORA scores between 0.55 and 0.74. The pelvis loading was influenced by the BMI (0.6) and sex (0.72). The cervical spine kinetics were affected by the fore-aft position (0.71), BMI (0.59), stature (0.74) and sex (0.73). The extremities' kinetics were sensitive to all tested parameters, with scores between 0.49 and 0.72 and between 0.39 and 0.58 for the lower and upper extremities, respectively.

TABLE F.II

FAR-SIDE CORA RESULTS – ALTERED RESPONSES ARE VISUALISED IN RED

	Kinematics								Kinetics				
	Pelvis	Spine (Lumbar)	Spine (Thoracic)	Spine (Cervical)	Torso	Head	Extremities Lower	Extremities Upper	Pelvis	Spine (Lumbar)	Spine (Cervical)	Extremities Lower	Extremities Upper
Backrest	0.93	0.95	0.90	0.89	0.92	0.88	0.86	0.71	0.85	0.93	0.82	0.72	0.58
Fore-Aft	0.83	0.83	0.81	0.84	0.85	0.82	0.72	0.59	0.77	0.89	0.71	0.50	0.46
BMI	0.62	0.53	0.61	0.70	0.77	0.73	0.65	0.55	0.60	0.77	0.59	0.52	0.39
Stature	0.88	0.91	0.88	0.89	0.91	0.90	0.71	0.69	0.77	0.90	0.74	0.49	0.54
Sex	0.87	0.93	0.90	0.93	0.92	0.90	0.80	0.74	0.72	0.86	0.73	0.64	0.58

Near-Side; Kinematic and Kinetic Patterns

In the Near-Side impact simulations, the occupant was generally subjected to low loads. Reclining the backrest to 30° reduced the head Y-speed by 0.2 m/s (-8%) and the lower neck magnitude of force by 0.1 kN (-23%). Similarly, when the seat was adjusted in the most rearward position, the head Y-speed was reduced by 0.4 m/s (-16%) compared to the nominal seat fore-aft position. In contrast, the lower neck force at the most forward position was increased by 0.1 kN (+37%) and the head Y-speed by 0.4 m/s (+13%). BMI influenced the pelvis lateral excursion as well as the lumbar spine and lower extremity kinetics. Compared to occupants of nominal BMI, underweight occupants were exposed to reduced (18 mm) pelvis Y-excursion, lumbar spine force and reduced (by 23 Nm, Fig. F.1) femur moment. Obese occupants were exposed to larger (26 mm) pelvis excursions, increased (+40%) lumbar spine force and extremity forces (Fig. F.1). The occupant's stature influenced the head kinematics; being 141 mm taller increased the head Y-rotation by 6° and the lower neck moment by 7 Nm. Additionally, increased (up to 0.5 kN, Fig. F.2) right upper tibia forces were recorded. Female occupants presented altered pelvis kinematic patterns, with 5° smaller peak pelvis rotation around the Z-axis and 8 mm less pelvis Y-excursion.

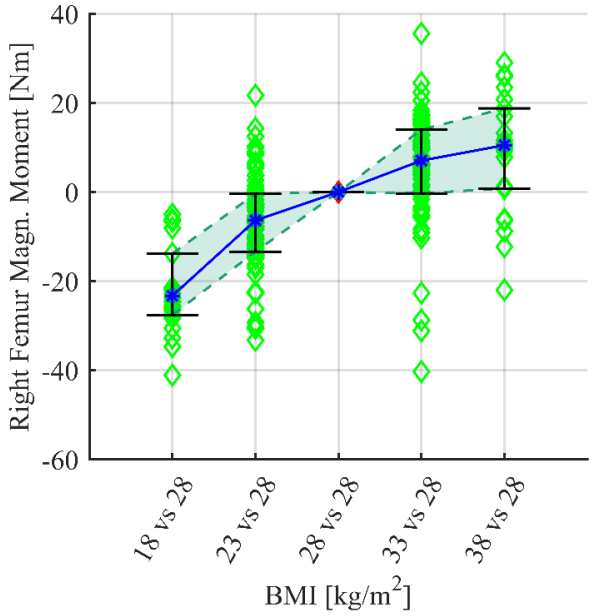

Fig. F.1. Influence of BMI on Right Femur magnitude of moment during the Near-Side impact simulations. A median reduction of 23 Nm can be seen for occupants with a BMI of 18 kg/m^2, and an increase of 10 Nm can be seen for occupants with a BMI of 38 kg/m^2, compared to occupants with nominal BMI (28 kg/m^2). The occupant responses are always compared between occupants of the same stature and sex, who are positioned in the seat adjustments.

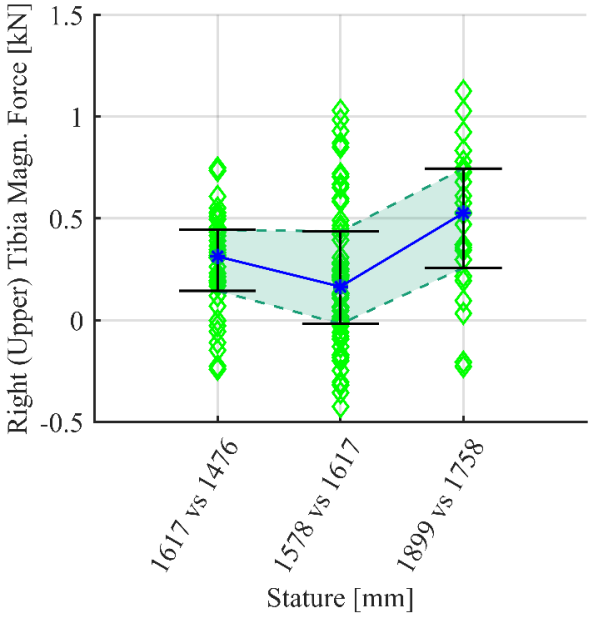

Fig. F.2. Right Tibia magnitude of force during the Near-Side impact simulations for occupants with non-nominal stature. Increasing the stature, in steps of 141 mm, increased the magnitude of force between 0.16 kN and 0.53 kN. Increasing from 1758 mm to 1899 mm had the largest effect, with a median increase of 0.53 kN.

Far-Side; Kinematic and Kinetic Patterns

Similar to the Near-Side impact simulations, the peak head relative Y-speed was reduced by 0.4 m/s (-7%) when the seat was adjusted in the most rearward position. Obese occupants were linked with increased lateral pelvis excursions (+27 mm) and loading in the pelvic region (+43%). On the other hand, reduced pelvis excursions and loading were observed for underweight occupants. On the contrary, the head of underweight occupants moved further inboard (+25 mm) with increased head rotations (+20°) around the X-axis, and the head of obese occupants moved (-30 mm) less inboard with reduced (-18°) head rotation, compared to occupants of nominal BMI. Additionally, a u-shape response between torso Z-rotation and BMI was observed; occupants with BMI diverging from nominal rotated more (18 kg/m^2 +2°, 38 kg/m^2 +5.8°). Increased lower extremity loading was observed for obese occupants, as well as for occupants with increased stature. Females were associated with lower pelvis lateral excursions compared to male occupants. However, the loading of the pelvis of females was generally increased. Additionally, the torso of the female occupants reached a higher (0.4 m/s) torso lateral speed and rotated 2.4° more around the Z-axis compared to males of the same stature and BMI during the Near-Side impact simulations.

Appendix G

KINEMATIC AND KINETIC SENSITIVITY ANALYSIS RESULTS

In Table G.I to Table G.IV, the median change of analysed response is reported, along with the IQR in parenthesis. Additionally, the percentage change is reported after the slash "/" punctuation. The result of the Wilcoxon signed rank test at $p \leq 0.05$ is symbolised with the asterisk "*" punctuation.

TABLE G.I
NEAR-SIDE

Backrest		30° vs. 25°		
Head	Head CoG Y-speed [m/s]	*-0.2 (-0.25,-0.16) / -8% (-9%,-6%)		
Spine (Cervical)	Lower Neck Magn. Force [kN]	*-0.1 (-0.17,-0.05) / -23% (-37%,-12%)		
Fore-aft		Full rearward vs. Nom.	Full forward vs. Nom.	
Head	Head CoG Y-speed [m/s]	*-0.41 (-0.46,-0.35) / -16% (-19%,-14%)	*0.33 (0.28,0.36) / 13% (11%,14%)	
Spine (Cervical)	Lower Neck Magn. Force [kN]	*-0.02 (-0.11,0.03) / -5% (-25.8%,6%)	*0.11 (0.07,0.23) / 38% (19%,85%)	
BMI		18 vs. 28	38 vs. 28	
Pelvis	Pelvis CoG Y-excursion [mm]	*-17 (-23,-13) / -21% (-25%,-17%)	*26 (23,29) / 31% (26%,37%)	
	Right SI Joint Magn. Force [kN]	*-0.12 (-0.22,-0.10) / -26% (-39.75%,-22%)	*0.26 (0.21,0.29) / 54% (43.92%,60%)	
	Right SI Joint Magn. Moment [Nm]	*-14 (-15,-12) / -44% (-49%,-37%)	*21 (17,27) / 69% (54%,100%)	
	Right ASIS Magn. Force [kN]	*0.07 (0.03,0.14) / 30% (12%,75%)	*0.08 (0.01,0.12) / 37% (3%,57%)	
Spine (Lumbar)	L5 Magn. Force [kN]	*-0.17 (-0.20,-0.09) / -34% (-36%,-21%)	*0.21 (0.12,0.29) / 40% (26%,62%)	
Spine (Cervical)	Lower Neck Magn. Moment [Nm]	*-4 (-12,-2) / -41% (-54%,-18%)	*20 (14,26) / 182% (94%,240%)	
Lower Extremities	Right Femur Magn. Force [kN]	*-0.08 (-0.16,0.00) / -19% (-28%,0%)	*0.25 (0.16,0.36) / 52% (28%,79%)	
	Right Femur Magn. Moment [Nm]	*-23 (-28,-14) / -41% (-49%,-31%)	*11 (1,19) / 18% (2%,39%)	
Upper Extremities	Right Lower Humerus Magn. Moment [Nm]	*-10 (-13,0) / -41% (-59%,-3%)	*6 (4,10) / 27% (14%,82%)	
	Right Lower Humerus Magn. Force [kN]	*0.04 (0.02,0.08) / 21% (8%,42%)	*0.16 (0.12,0.19) / 75% (51%,111%)	
Stature		1617 vs. 1476	1758 vs. 1617	1899 vs. 1758
Head	Head Y-rotation [°]	*3.6 (0.7,7.3) / 50% (6%,86%)	*6.3 (3.1,9.7) / 68% (40%,93%)	*6.4 (2.9,9.2) / 49% (19%,91%)
Spine (Cervical)	Lower Neck Magn. Moment [Nm]	*-5 (-12,-3) / -37% (-53%,-19%)	*7 (1,12) / 54% (14%,92%)	*7(3,10) / 28% (9%,92%)
Lower Extremities	Right Upper Tibia Magn. Force [kN]	*0.31 (0.14,0.44) / 87% (40%,123%)	*0.16 (-0.02,0.44) / 27% (-2%,63%)	*0.53 (0.26,0.74) / 69% (28%,111%)
Sex		Female vs. Male		
Pelvis	Pelvis Z-rotation [°]	*-5.1 (-6.1,-2.9) / -42% (-56%,-27%)		
	Pelvis CoG Y-excursion [mm]	*-8 (-10,-3) / -8% (-11%,-3%)		
Spine (Lumbar)	L5 Magn. Force [kN]	*0.09 (0.06,0.11) / 19% (13%,28%)		

TABLE G.II
FAR-SIDE

Backrest			30° vs. 25°		
Upper Extremities	Left Lower Humerus Magn. Force [kN]		*-0.11 (-0.18,-0.05) / -23% (-38%,-15%)		
	Left Forearm Magn. Force [kN]		*-0.08 (-0.17,-0.01) / -17% (-35%,-2%)		
Fore-aft			Full rearward vs. Nom.	Full forward vs. Nom.	
Head	Head CoG Y-speed [m/s]		*-0.41 (-0.51,-0.23) / -7% (-9%,-4%)	*0.34 (0.30,0.38) / 6% (5%,7%)	
	Head CoG Y-excursion [mm]		*-20 (-32,-13) / -6% (-9%,-4%)	*8 (-1,11) / 3% (0%,4%)	
Upper Extremities	Left Lower Humerus Magn. Force [kN]		*-0.14 (-0.25,-0.02) / -34% (-45%,-8%)	*0.05 (0.00,0.16) / 18% (1%,43%)	
BMI			18 vs. 28	38 vs. 28	
Pelvis	Pelvis CoG Y-excursion [mm]		*-34 (-48,-31) / -33% (-42%,-31%)	*27 (19,46) / 24% (17%,37%)	
	Interaction with Sex	Female	*-32 (-34,-29) / -32% (-33%,-29%)	*21 (9,30) / 22% (8%,31%)	
		Male	*-49 (-53,-47) / -42% (-45%,-40%)	*43 (26,49) / 38% (23%,41%)	
	Left Pubic Rami Magn. Force [kN]		*-0.29 (-0.35,-0.22) / -26% (-30%,-18%)	*0.08 (0.01,0.27) / 7% (1%,22%)	
	Left SI Joint Magn. Force [kN]		*-0.27 (-0.37,-0.24) / -23% (-26%,-20%)	*0.57 (0.42,0.78) / 43% (31%,67%)	
	Right SI Joint Magn. Force [kN]		*-0.52 (-0.58,-0.44) / -42% (-45%,-35%)	*0.31 (0.14,0.51) / 27% (13%,38%)	
Torso	Sternum Y-speed [m/s]		*-0.30 (-0.52,-0.15) / -8% (-13%,-4%)	-0.06 (-0.29,0.31) / -2% (-8%,9%)	
	Sternum Y-excursion [mm]		*-17 (-18,-12) / -12% (-12%,-9%)	*6 (2,15) / 4% (1%,12%)	
Head	Head CoG Y-excursion [mm]		*25 (16,33) / 8% (5%,10%)	*-30 (-43,-18) / -10% (-14%,-6%)	
	Head X-rotation [°]		*19.8 (11.2,21.7) / 25% (13%,27%)	*-17.5 (-21.3,-11.2) / -21% (-25%,-15%)	
Lower Extremities	Left Femur Magn. Force [kN]		*-0.29 (-0.35,-0.15) / -32% (-35%,-18%)	*0.51 (-0.01,0.68) / 49% (-1%,76%)	
	Left Lower Tibia Magn. Force [kN]		*0.19 (0.10,0.34) / 34% (18%,61%)	*0.82 (0.51,1.13) / 82% (47%,135%)	
Stature			1617 vs. 1476	1758 vs. 1617	1899 vs. 1758
Lower Extremities	Left Lower Tibia Magn. Force [kN]		*0.19 (0.10,0.34) / 34% (18%,61%)	*0.34 (0.17,0.89) / 53% (28%,102%)	*0.82 (0.51,1.13) / 82% (47%,135%)
	Left Femur Magn. Force [kN]		0.04 (-0.07,0.11) / 3% (-7%,14.62%)	*0.18 (0.06,0.31) / 21% (7%,37%)	*0.30 (0.14,0.47) / 31% (16%,46%)
Sex			Female vs. Male		
Pelvis	Pelvis CoG Y-excursion [mm]		*-8 (-12,-2) / -7% (-10%,-2%)		
	Left SI Joint Magn. Force [kN]		*0.36 (0.28,0.43) / 33% (25%,40%)		
	Right SI Joint Magn. Force [kN]		*0.09 (0.02,0.19) / 8% (1.71%,16%)		
Torso	Sternum Y-speed [m/s]		*0.41 (0.33,0.48) / 12% (9%,13%)		
	Torso Z-rotation [°]		*2.4 (-0.4,4)		
Spine (Lumbar)	L5 Magn. Force [kN]		*0.20 (0.11,0.33) / 20% (9%,35%)		
Spine (Cervical)	Lower Neck Magn. Moment [Nm]		*-9 (-14,-7) / -12% (-17%,-9%)		

TABLE G.III
INTERSECTION FRONTAL

Backrest			30° vs. 25°	
Torso	Sternum X-speed [m/s]		*0.27 (0.2,0.32) / 11% (7%,14%)	
Head	Head CoG X-speed [m/s]		*0.28 (0.18,0.36) / 6% (4%,7%)	
Fore-aft			Full rearward vs. Nom.	Full forward vs. Nom.
Pelvis	Pelvis CoG X-excursion [mm]		*7(3,13) / 9% (3%,18%)	0 (-6,5) / -1% (-7%,5%)
	Pelvis Y-rotation [°]		*7.9 (5.7,12.1)	*-1.9 (-3.7,-0.7)
	Interaction with BMI	18 kg/m²	14.2 (12,15.4)	-0.9 (-2.1,0.4)
		23 kg/m²	*10.1 (7.8,12.9)	*-2.4 (-3.7,-1.7)
		33 kg/m²	*6.4 (4.2,8.7)	-2.6 (-4.1,-0.5)
		38 kg/m²	5 (4,6.2)	0 (-0.6,0.6)
	Interaction with Stature	1476 mm	*12.5 (11.3,13.9)	-2.9 (-4.1,-0.9)
		1617 mm	*11.9 (7.4,13.9)	*-1.9 (-3.1,-0.6)
		1758 mm	*5.4 (3.7,7.6)	-/- (Occupant cannot fit)

	Right ASIS Magn. Force [kN]		*0.18 (0.10,0.45) / 24% (15%,70%)	*-0.14 (-0.29,-0.10) / -21% (-37%,-16%)
	Left ASIS Magn. Force [kN]		*0.18 (0.07,0.30) / 21% (8%,35%)	*-0.15 (-0.20,-0.00) / -18% (-24%,-0%)
Torso	Sternum X-speed [m/s]		*0.39 (0.32,0.48) / 16% (12%,19%)	*-0.32 (-0.44,-0.24) / -15% (-18%,-11%)
Spine (Lumbar)	L1 Magn. Force [kN]		*0.20 (0.15,0.25) / 25% (18%,34%)	*-0.22 (-0.27,-0.17) / -29% (-35%,-21%)
Head	Head CoG X-speed [m/s]		*0.47 (0.33,0.62) / 9% (6.64%,12.75%)	*-0.32 (-0.51,-0.24) / -6% (-10%,-5%)
Lower Extremities	Right Femur Magn. Force [kN]		0.17 (-0.24,0.46) / 25% (-20%,99%)	-0.16 (-0.41,0.31) / -21% (-69%,64%)
	Interaction with BMI	18 kg/m²	0.29 (0.03,0.57) / 136% (5%,274%)	-0.40 (-0.41,-0.40) / -74% (-74%,-73%)
		23 kg/m²	0.07 (0.03,0.62) / 10% (-3%,204%)	-0.54 (-0.54,-0.04) / -69% (-71%,-6%)
		33 kg/m²	0.01 (-0.74,0.26) / 1% (-44%,50%)	0.39 (-0.29,0.75) / 88% (-40%,140%)
		38 kg/m²	-0.34 (-1.13,0.48) / -18% (-61%,105%)	1.23 (1.12,1.34) / 271% (244%,299%)
	Interaction with Stature	1617 mm	*0.20 (0.04,0.38) / 36% (6%,88%)	-0.17 (-0.47,0.61) / -32% (-70%,-126%)
		1899 mm	*-1.18 (-1.52,-0.8) / -68% (-70%,-59%)	-/- (Occupant cannot fit)
	Left Femur Magn. Force [kN]		0.02 (-0.12,0.21) / 2% (-24%,61%)	*-0.21 (-0.27,-0.09) / -31% (-36%,-22%)
	Right Femur Magn. Moment [Nm]		*29 (19,36) / 80% (34%,125%)	*-19 (-27,-14) / -46% (-54%,-31%)
	Left Femur Magn. Moment [Nm]		*20 (11,29) / 55% (26%,105%)	*-16 (-23,-10) / -41% (-52%,-26%)
	Right Lower Tibia Magn. Force [kN]		*0.51 (0.11,0.61) / 72% (33%,100%)	*-0.22 (-0.50,-0.11) / -44% (-57%,-29%)
	Left Lower Tibia Magn. Force [kN]		*0.57 (0.06,0.77) / 76.77% (18%,123%)	*-0.19 (-0.47,-0.13) / -44% (-66%,-35%)
	Interaction with BMI	18 kg/m²	-0.03 (-0.1,0.05) / -0% (-25%,32%)	0.24 (0.22,0.25) / 146% (146%,147%)
		38 kg/m²	-0.7 (-0.95,-0.58) / -60% (-65%,-58%)	0.84 (0.72,0.96) / 86% (69%,103%)
BMI			18 vs. 28	38 vs. 28
Pelvis	Pelvis CoG X-excursion [mm]		*-34 (-36,-29) / -38% (-40%,-35%)	*24 (14,31) / 26% (15%,35%)
	Pelvis Y-rotation [°]		-0.6 (-2.4,0.9)	0.9 (-1.5,1.8)
Torso	Sternum X-speed [m/s]		*-0.11 (-0.24,-0.04) / -4% (-10%,-2%)	*0.24 (0.16,0.32) / 10% (6%,13%)
	Torso Z-rotation [°]		0 (-2.3,7)	*6.9 (5.9,8.9)
	Interaction with Sex	Male	*7.55 (4.63,9.26) / 271% (98%,332%)	*7.78 (5.95,9.54) / 264% (144%,364%)
		Female	*-1.8 (-3.09,-0.82) / -24% (-46%,-13%)	*6.59 (5.02,7.96) / 100% (68%,141%)

Stature			1617 vs. 1476	1758 vs. 1617	1899 vs. 1758
Pelvis	Pelvis Y-rotation [°]		*-1.6 (-3,1)	*2.8 (-0.3,5)	*4.5 (3.1,6)
Lower Extremities	Right Lower Tibia Magn. Force [kN]		*0.13 (0.07,0.34) / 57% (32%,111%)	*0.25 (0.14,0.46) / 65% (38%,101%)	*0.34 (0.20,0.51) / 41% (29%,92%)
	Left Lower Tibia Magn. Force [kN]		*0.12 (0.09,0.34) / 55% (43%,159%)	*0.28 (0.15,0.57) / 78% (45%,156%)	*0.44 (0.27,0.59) / 61% (38%,124%)
	Right Lower Tibia Magn. Moment [Nm]		-1 (-3,3) / -9% (-26%,54%)	*5 (2,10) / 59% (19%,121%)	*8 (4,19) / 63% (32%,144%)
	Left Lower Tibia Magn. Moment [Nm]		*2 (1,4) / 20% (6%,49%)	*3 (1,6) / 25% (10%,55%)	*4 (2,8) / 30% (14%,42%)
Sex			Female vs. Male		
Pelvis	Pelvis Y-rotation [°]		*7.6 (6.1,9.2)		
	(Init. Pelvis Y-rotation [°])		*7.4 (6.2,8.5)		

TABLE G.IV

ONCOMING FRONTAL

Backrest			30° vs. 25°
Pelvis	Pelvis Y-rotation [°]		*4.4 (1.4,6.7)
	Interaction with stature	1476 mm	0.3 (-2.7,3)
		1617 mm	*3.9 (1.40,5.9)
	(Init. Pelvis Y-rotation [°])		*3.8 (3.3,4.1)
	Right SI Joint Magn. Force [kN]		*0.19 (0.08,0.41) / 12% (5%,20%)
	Right ASIS Magn. Force [kN]		*0.08 (-0.03,0.22) / 3% (-1%,9%)
Spine (Lumbar)	L1 Magn. Force [kN]		*0.37 (0.20,0.52) / 17% (11%,25%)
	L5 Magn. Force [kN]		*0.30 (0.15,0.45) / 21% (12%,31%)
Spine (Cervical)	Lower Neck Magn. Force [kN]		*0.24 (0.06,0.40) / 17% (4%,26%)

Fore-aft			Full rearward vs. Nom.	Full forward vs. Nom.
Pelvis	Pelvis CoG X-excursion [mm]		*29(13,70) / 17% (9%,44%)	*-24 (-37,-45) / -15% (-20%,-4%)
	Pelvis Y-rotation [°]		*7 (3,11)	*-7.5 (-10.7,-5.6)
	Interaction with BMI	18 kg/m²	19.4 (16.4,22.9)	-12.9 (-13,-12.7)
		38 kg/m²	5.6 (1.6,7.7)	-8.8 (-9.5,-8)

	Interaction with stature	1476 mm	*15.3 (11,16.7)	-5.6 (-7.1,-5.1)
		1617 mm	*9.2 (4.0,11.5)	*-8.5 (-11.9,-6.4)
		1758 mm	3.3 (-1.1,9.1)	-/- (Occupant cannot fit)
		1899 mm	5 (0,5.1)	-/- (Occupant cannot fit)
	Right ASIS Magn. Force [kN]		*1.11 (0.68,1.66) / 51% (29%,93%)	*-0.82 (-1.05,-0.65) / -33% (-45%,-25%)
	Left ASIS Magn. Force [kN]		*0.86 (0.60,1.12) / 42% (27%,60%)	*-0.68 (-0.81,-0.48) / -29% (-34%,-23%)
	Right SI Joint Magn. Force [kN]		*0.63 (0.47,0.97) / 41% (29%,63%)	*-0.6 (-0.7,-0.38) / -30% (-37%,-21%)
	Left SI Joint Magn. Force [kN]		*0.58 (0.36,0.75) / 36% (21%,47%)	*-0.42 (-0.58,-0.26) / -25% (-31%,-19%)
Torso	Sternum res-speed [m/s]		*0.59 (0.39,0.72) / 8% (6%,10%)	*-0.68 (-0.84,-0.36) / -10% (-12%,-6%)
Spine (Lumbar)	L1 Magn. Force [kN]		*1.46 (1.16,1.63) / 77% (60%,88%)	*-0.64 (-0.89,-0.47) / -37% (-42%,-32%)
	L5 Magn. Force [kN]		*1.03 (0.83,1.21) / 74% (57%,101%)	*-0.38 (-0.51,-0.09) / -30% (-34%,-10%)
Spine (Cervical)	Lower Neck Magn. Force [kN]		*0.32 (-0.04,0.63) / 18% (-2%,44%)	*-0.15 (-0.32,-0.08) / -13% (-25%,-4%)
	Lower Neck Magn. Moment [Nm]		*13 (-17,33) / 13% (-16%,54%)	*-15 (-27,-7) / -18% (-25%,-12%)
Head	Head CoG res-speed [m/s]		*2.21 (1.86,2.51) / 18% (15%,22%)	*-2.44 (-2.80,-2.23) / -21% (-25%,-18%)
Lower Extremities	Right Femur Magn. Force [kN]		0.41 (-0.79,0.94) / 34% (-39%,87%)	0.31 (-0.52,0.81) / 19% (-42%,79%)
	Interaction with BMI	18 kg/m^2	0.69 (0.36,1.07) / 88% (35%,153%)	-0.6 (-0.64,-0.58) / -58% (-60%,-55%)
		38 kg/m^2	-1.56 (-2.7,-0.13) / -44% (-66%,-4%)	1.05 (0.46,1.64) / 64% (21%,106%)
	Interaction with stature	1476 mm	0.53 (0.29,0.71) / 35% (18%,54%)	-0.25 (-0.57,0.15) / -17% (-34%,10%)
		1899 mm	*-0.8 (-1.38,-0.71)/ -35% (-44%,-24%)	-/- (Occupant cannot fit)
	Left Femur Magn. Force [kN]		0.17 (-0.47,0.64) / 14% (-25%,78%)	-0.19 (-0.69,0.76) / -16% (-46%,82%)
	Interaction with BMI	18 kg/m^2	0.43 (0.06,0.86) / 65% (5%,158%)	-0.82 (-0.9,-0.74) / -68% (-72,-63%)
		38 kg/m^2	-0.35 (-1.29,0.65) / -4% (-45%,68%)	1.53 (1.32,1.75) / 152% (112%,193%)
	Interaction with stature	1476 mm	0.15 (0.04,0.29) / 12% (2%,22%)	*-0.69 (-0.89,-0.63) / -48% (-59%,-47%)
		1899 mm	*-1.07 (-1.36,-0.71)/ -42% (-50%,-26%)	-/- (Occupant cannot fit)
	Right Femur Magn. Moment [Nm]		*46 (33,75) / 58% (39%,101%)	*-27(-36,-2) / -38% (-45%,-4%)
	Left Femur Magn. Moment [Nm]		*29 (19,45) / 32% (21%,55%)	*-39 (-44,-27) / -41% (-49%,-35%)
	Left Lower Tibia Magn. Force [kN]		*-0.70 (-1.12,-0.32) / -28% (-56%,-16%)	*0.99 (0.72,1.25) / 74% (56%,157%)
	Right Lower Tibia Magn. Force [kN]		*-0.41 (-0.89,-0.10) / -26% (-34%,-8%)	*0.84 (0.48,1.02) / 58% (38%,75%)
BMI			18 vs. 28	38 vs. 28
Pelvis	Pelvis CoG X-excursion [mm]		*-72 (-79,-58) / -39% (-41%,-34%)	*18 (7,43) / 10% (5%,23%)
	Interaction with fore-aft	Full rearward	-89 (-92,-86) / -42% (-44%,-42%)	45 (28,53) / 22% (13%,26%)
		Full Forward	-33 (-35,-30) / -23% (-25%,-22%)	6 (0,12) / 4% (0%,8%)
	Pelvis Y-rotation [°]		*7.8 (-1.7,13.7)	*5.6 (1,8.6)
	Interaction with sex	Female	-1.29 (-5.47,9.02)	*8.53 (6.77,12.58)
		Male	*10.02 (7.93,13.72)	1.96 (-1.23,5.08)
	Interaction with fore-aft	Full rearward	15.78 (14.6,17.45)	6.49 (-2.54,16.95)
		Full Forward	-11.77 (-13.64,-9.9)	7 (5.56,8.44)
	Right ASIS Magn. Force [kN]		*-0.54 (-0.89,-0.34) / -18% (-26%,-13%)	*-0.32 (-0.49,-0.08) / -14% (-23%,-3%)
	Left ASIS Magn. Force [kN]		*-0.41 (-0.51,-0.21) / -17% (-20%,-8%)	*-0.37 (-0.58,-0.16) / -15.51% (-22%,-8%)
	Right Pubic Rami Magn. Force [kN]		*0.25 (-0.08,0.63) / 19% (-5%,52%)	*-0.3 (-0.5,-0.16) / -22% (-35%,-15%)
	Left Pubic Rami Magn. Force [kN]		0.01 (-0.07,0.13) / 1% (-9%,17%)	*-0.17 (-0.31,-0.05) / -20% (-27%,-7%)
	Right SI Joint Magn. Force [kN]		*-0.81 (-1.19,-0.56) / -40% (-47%,-32%)	-0.05 (-0.34,0.21) / -3% (-17%,12%)
	Left SI Joint Magn. Force [kN]		*-0.33 (-0.52,-0.27) / -20% (-25%,-14%)	0.12 (-0.14,0.28) / 6% (-6%,17%)
Torso	Sternum res-speed [m/s]		*-0.76 (-0.85,-0.68) / -10% (-13%,-9%)	*0.46 (0.11,0.59) / 7% (2%,8%)
Spine (Lumbar)	L1 Magn. Force [kN]		*-0.41 (-0.51,-0.21) / -17% (-20%,-8%)	*-0.37 (-0.58,-0.16) / -16% (-22%,-8%)
	L5 Magn. Force [kN]		*-0.38 (-0.87,-0.10) / -24% (-36%,-8%)	-0.11 (-0.35,0.06) / -7% (-18%,6%)
Spine (Cervical)	Lower Neck Magn. Force [kN]		*0.20 (-0.14,0.43) / 14% (-10%,30%)	*0.90 (0.66,1.38) / 76% (52%,89%)
	Lower Neck Magn. Moment [Nm]		*-21 (-32,-9) / -26% (-37%,-11%)	*78 (63,118) / 107% (87%,138%)

Head	Head CoG res-speed [m/s]		*0.14 (0.03,0.22) / 1% (0%,2%)	*-0.15 (-0.29,-0.06) / -1% (-3%,0%)	
	Head Z-rotation [°]		*13.2 (11,16) / 75% (60%,107%)	-3.5 (-6.3,0.8) / -18% (-35%,7%)	
Lower Extremities	Right Femur Magn. Force [kN]		*-0.20 (-1.10,0.10) / -14% (-61%,9%)	*1.14 (0.23,1.55) / 69% (20%,118%)	
	Left Femur Magn. Force [kN]		*-0.21 (-0.67,0.05) / -18% (-51%,4%)	*0.81 (0.07,1.38) / 67% (7%,107%)	
	Right Femur Magn. Moment [Nm]		*-9 (-19,0) / -14% (-24%,1%)	*5 (0,33) / 6% (0%,34%)	
	Left Femur Magn. Moment [Nm]		*-43 (-57,-32) / -46% (-52%,-40%)	*19 (4,30) / 17% (3%,34%)	
	Right Lower Tibia Magn. Force [kN]		*-0.77 (-1.65,-0.63) / -53% (-72%,-47%)	*1.27 (1.05,1.84) / 86% (42%,106%)	
	Left Lower Tibia Magn. Force [kN]		*-1.71 (-1.97,-0.93) / -67% (-76%,-57%)	*1.04 (0.86,1.39) / 46% (32%,110%)	
Stature			1617 vs. 1476	1758 vs. 1617	1899 vs. 1758
Pelvis	Pelvis Y-rotation [°]		*9.1 (5.8,11.5)	*6.4 (2.8,11)	*8.1 (6.3,11.1)
	Interaction with Sex	Female	*9.1 (5.8,11.4)	*9.8 (6,14.7)	Not applicable
		Male	Not applicable	*3.3 (1.5,7.3)	*8.1 (6.2,11.1)
	Right ASIS Magn. Force [kN]		0.01 (-0.25,0.21) / 0% (-11%,7%)	*-0.13 (-0.72,0.07) / -4% (-30%,2%)	*-0.64 (-0.73,-0.25) / -25% (-27%,-8%)
	Left ASIS Magn. Force [kN]		*-0.12 (-0.41,0.09) / -5% (-19%,4%)	*-0.11 (-0.34,0.11) / -3% (-14%,5%)	*-0.19 (-0.36,0.07) / -7% (-17%,3%)
Torso	Sternum res-speed [m/s]		*0.67 (0.49,0.75) / 11% (8%,13%)	*0.37 (0.25,0.52) / 5% (4%,8%)	*0.43 (0.35,0.48) / 5% (5%,6%)
Spine (Lumbar)	L1 Magn. Force [kN]		*-0.19 (-0.35,0.07) / -10% (-17%,2%)	*0.19 (0.05,0.37) / 9% (1%,20%)	*0.39 (0.21,0.54) / 16% (7%,23%)
	L5 Magn. Force [kN]		*-0.16 (-0.26,0.04) / -11% (-17%,2%)	*0.18 (-0.01,0.34) / 16% (-0%,30%)	*0.44 (0.22,0.59) / 26% (13%,38%)
Spine (Cervical)	Lower Neck Magn. Force [kN]		*-0.08 (-0.18,0.02) / -6% (-11%,2%)	*0.08 (-0.02,0.22) / 5% (-1%,16%)	*0.31 (-0.09,0.61) / 18% (-4%,39%)
Head	Head CoG res-speed [m/s]		*0.49 (0.41,0.57) / 4% (4%,5%)	*0.48 (0.38,0.63) / 4% (3%,5%)	*0.57 (0.41,0.84) / 4% (3%,6%)
Lower Extremities	Right Femur Magn. Force [kN]		-0.16 (-0.37,0.31) / -11% (-26%,18%)	*-0.18 (-0.56,1.25) / -14% (-32%,102%)	*0.93 (0.48,1.55) / 70% (19%,135%)
	Left Femur Magn. Force [kN]		0.03 (-0.32,0.28) / 2% (-21%,22%)	-0.09 (-0.44,0.77) / -6% (-32%,89%)	*1.14 (0.42,1.45) / 86% (33%,131%)
	Right Femur Magn. Moment [Nm]		*-20 (-37,-1) / -19% (-40%,-1%)	*-14 (-38,10) / -10% (-28%,14%)	*26 (14,34) / 25% (13%,41%)
	Left Femur Magn. Moment [Nm]		*8 (-2,20) / 8% (-2%,27%)	*-8 (-18,6) / -7% (-15%,6%)	-3 (-18,8) / -2% (-15%,8%)
	Right Lower Tibia Magn. Force [kN]		*0.57 (0.18,0.71) / 43% (20%,78%)	*0.67 (0.39,0.98) / 56% (25%,79%)	*0.17 (-0.10,0.65) / 10% (-4%,51%)
	Left Lower Tibia Magn. Force [kN]		*0.85 (0.20,1.29) / 114.62% (46%,180%)	*1.30 (0.91,1.57) / 113% (63%,224%)	*0.36 (0.13,0.76) / 16% (5%,32%)
Sex			Female vs. Male		
Pelvis	Pelvis Y-rotation [°]		0.8 (-3.9,6.3)		
	(Init. Pelvis Y-rotation [°])		*7.4 (6.2,8.5)		
	Right ASIS Magn. Force [kN]		*0.22 (-0.07,0.37) / 8% (-3%,14%)		
	Left ASIS Magn. Force [kN]		*0.14 (-0.02,0.28) / 6% (-1%,12%)		
	Right SI Joint Magn. Force [kN]		*0.21 (0.00,0.42) / 11% (0%,20%)		
	Left SI Joint Magn. Force [kN]		*0.33 (0.24,0.45) / 21% (13%,26%)		
Torso	Sternum res-speed [m/s]		*-0.28 (-0.37,-0.21) / -4% (-5%,-3%)		
Spine (Lumbar)	L1 Magn. Force [kN]		*0.13 (0.06,0.27) / 7% (2%,14%)		
	L5 Magn. Force [kN]		*0.33 (0.23,0.45) / 25% (15%,33%)		
Spine (Cervical)	Lower Neck Magn. Force [kN]		*-0.26 (-0.54,0.01) / -17% (-27%,1%)		
	Lower Neck Magn. Moment [Nm]		*-35(-58,-12) / -32% (-41%,-19%)		

ERRATUM

The Influence of Occupant's Size, Shape and Seat Adjustment in Frontal and Side Impacts

Alexandros Leledakis, Jonas Östh, Johan Iraeus, Johan Davidsson, Lotta Jakobsson

The vehicle motion during Oncoming Frontal crash was not visible in Figure 2 in the first version of the manuscript. Additionally, we apologize for the misprinted legend labels in Figure A.2 (Appendix A), which made it difficult to distinguish the 10%, 50%, and 90% iso-probability lines. The updated figures can be found below.

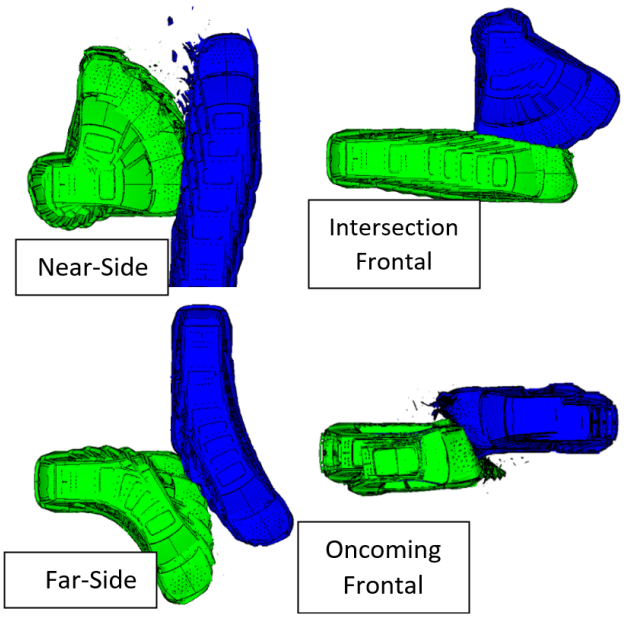

Fig. 2. Vehicle motion of the car-car impact. During the crash simulations, the HBM is located in the front passenger (right) seat of the host vehicle (green).

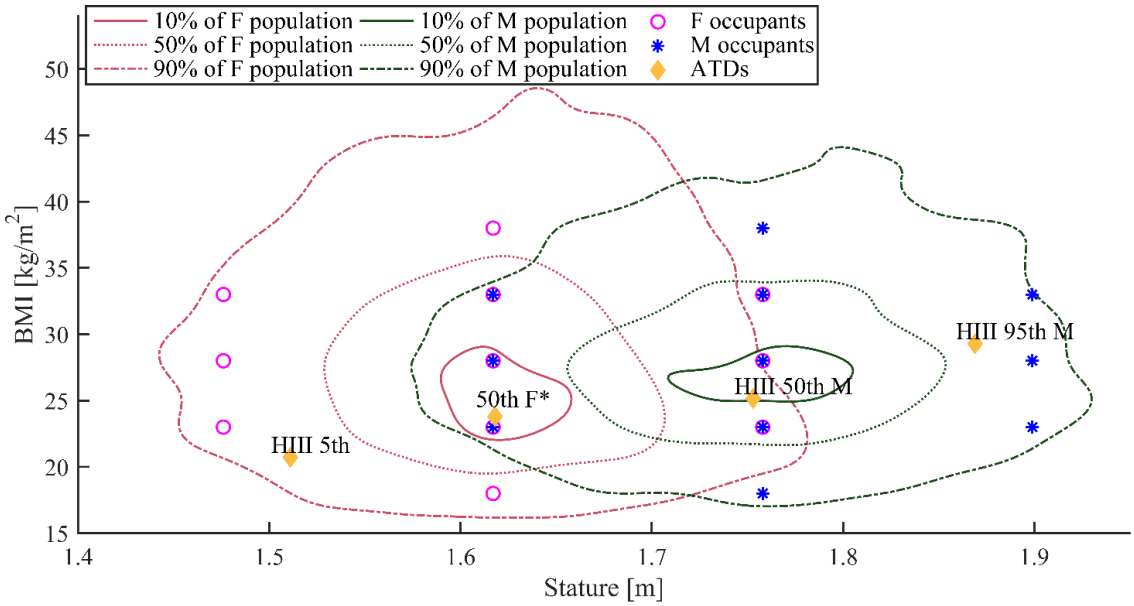

Fig. A.2. The bivariate distribution of the US population is illustrated using iso-probability contours lines for the female (in red) and male (in green) subpopulations. The contour lines define the borders that contain 10% (solid line), 50% (dotted line) and 90% of the subpopulations. The selected occupant sizes (BMI and stature) are visualised with magenta and circles and blue stars for the female and male populations. Additionally, the dimensions of the Hybrid-III Anthropomorphic Test Devices and the 50th percentile female in accordance with Schneider *et al.* [56] are included in yellow diamonds for easy comparison with the selected anthropometries.